HIGH FREQUENCY POUND-DREVER-HALL

OPTICAL RING RESONATOR SENSING

A Thesis

by

JAMES PAUL CHAMBERS

Submitted to the Office of Graduate Studies of
Texas A&M University
in partial fulfillment of the requirements for the degree of

MASTER OF SCIENCE

December 2007

Major Subject: Electrical Engineering

HIGH FREQUENCY POUND-DREVER-HALL

OPTICAL RING RESONATOR SENSING

A Thesis

by

JAMES PAUL CHAMBERS

Submitted to the Office of Graduate Studies of
Texas A&M University
in partial fulfillment of the requirements for the degree of

MASTER OF SCIENCE

Approved by:

Chair of Committee,	Christi K. Madsen
Committee Members,	Philip Hemmer
	Robert Nevels
	Edward Fry
Head of Department,	Costas Georghiades

December 2007

Major Subject: Electrical Engineering

ABSTRACT

High Frequency Pound-Drever-Hall
Ring Resonator Optical Sensing. (December 2007)
James Paul Chambers, B.S., Colorado School of Mines
Chair of Advisory Committee: Dr. Christi K. Madsen

A procedure is introduced for increasing the sensitivity of measurements in integrated ring resonators beyond what has been previously accomplished. This is demonstrated by a high-frequency, phase sensitive lock to the ring resonators. A prototyped fiber Fabry-Perot cavity is used for comparison of the method to a similar cavity. The Pound-Drever-Hall (PDH) method is used as a proven, ultra-sensitive method with the exploration of a much higher frequency modulation than has been previously discussed to overcome comparatively low finesse of the ring resonator cavities. The high frequency facilitates the use of the same modulation signal to separately probe the phase information of different integrated ring resonators with quality factors of 8.2 x10^5 and 2.4 x10^5.

The large free spectral range of small cavities and low finesse provides a challenge to sensing and locking the long-term stability of diode lasers due to small dynamic range and signal-to-noise ratios. These can be accommodated for by a calculated increase in modulation frequency using the PDH approach. Further, cavity design parameters will be shown to have a significant affect on the resolution of the phase-sensing approach. A distributed feedback laser is locked to a ring resonator to demonstrate the present sensitivity which can then be discussed in comparison to other fiber and integrated sensors.

The relationship of the signal-to-noise ratio (S/N) and frequency range to the cavity error signal will be explored with an algorithm to optimize this relationship. The free spectral range and the cavity transfer function coefficients provide input parameters to this relationship to determine the optimum S/N and frequency range of the respective cavities used for locking and sensing. The purpose is to show how future contributions to

the measurements and experiments of micro-cavities, specifically ring resonators, is well-served by the PDH method with high-frequency modulation.

ACKNOWLEDGEMENTS

Though there are countless individuals who helped me reach this far, there are specific ones that made this leg of the journey possible. First thanks to God, for the opportunities and challenges of life. My wife, Valerie, for finding great worth in the inevitable sharing of patience and determination. Dr. Christi Madsen, Donnie Adams, and Mehmet Solmaz for the many encouraging and informative discussions. And great thanks to the rest of my committee, Drs. Philip Hemmer, Robert Nevels and Ed Fry, without whom the worth of this effort would have been greatly lessened. Lastly, to my parents and other family who have believed in my decisions, come what may.
Thanks.

TABLE OF CONTENTS

Page

LIST OF FIGURES

FIGURE Page

FIGURE Page

LIST OF TABLES

1. INTRODUCTION

This thesis establishes a procedure for increasing the sensitivity of measurements in ring resonator cavities beyond what has been previously accomplished. This is achieved by a high-frequency phase-modulation lock to an integrated ring resonator. A prototyped fiber Fabry-Perot (FP) cavity is fabricated to compare the cavity response of a ring resonator to a widely utilized cavity type. The Pound-Drever-Hall (PDH) method is used as a proven, ultra-sensitive method with the exploration of a much higher frequency modulation than has been previously discussed to overcome comparatively low finesse of the ring resonator cavities. The high frequency facilitates the use of the same modulation signal to separately probe the phase information of different integrated ring resonators with quality factors of 8.2×10^5 and 2.4×10^5.

The large free spectral range (FSR) of small cavities provides a challenge to locking and sensing due to the small signal-to-noise ratio (S/N) and the dynamic frequency range of the cavities. These challenges can be partly overcome by a calculated increase in the phase modulation frequency. The laser in this experiment is locked to one ring resonator while another ring resonator is tuned around resonance to demonstrate the cavity sensitivity. The sensitivity of these integrated ring cavities can then be compared to other fiber or integrated temperature, strain, biological, and environmental sensors.

Lastly, the relationship of the frequency range and S/N ratio to the cavity error signal is explored with an algorithm to optimize this relationship using the modulation frequency. The FSR and the loss of the cavity provide input parameters to this relationship to determine the optimum S/N ratio and dynamic range of the respective cavities used for locking and sensing. The purpose is to show how future contributions to the measurements and experiments of micro-cavities, specifically ring resonators, are enhanced by the PDH method with a high-frequency phase modulation.

This thesis follows the style of *Journal of Lightwave Technology*.

Optical Cavity Sensing

Optical cavities have been used as stable references for locking and sensing the frequency of lasers for the past forty years. The use of optical cavities to detect the frequency of light is detailed by White [1], where the method used is similar to microwave frequency discrimination first proposed by Pound [2]. The feedback from the experiment was able to stabilize 0.1 to 1Hz frequency fluctuations of a gas laser. This work would be greatly expanded by others including Drever and Hall [3] who developed in subsequent work a method to sample the phase of the optical device around resonance.

More recently, there have been numerous papers for obtaining locks of a laser frequency using gas absorption and interferometer cavities [4]. Cavity locking has been accomplished by locking to a more stable laser [5] and laser stability has been shown frequency-locked to less than 1 hertz variation for accurate time referencing applications [6, 7]. Optical sensing has also been accomplished through many similar methods [8]. However as the size of devices decrease, there become further limitations in device design and methods to sense frequency. While theoretical results are comparable, present sensing using micro-cavities [9, 10, 11] has shown less resolution and accuracy compared to larger cavities [12].

Because of their integrated design and mix of frequency range and finesse, ring resonators are an excellent choice for small, easily packaged, and low-cost sensing cavities. Also, single or multiple ring resonators can be scaled in size and parameters to the detection resolution of the intended medium. In this paper, the response for a single ring will be optimized for feedback- but the math can be scaled with further transfer functions to include a number of rings and receive a more complex response. The sections on optical filters and optical devices will discuss how the design of a ring resonator determines the suited purpose.

Most micro-cavities, including ring resonators [9] and microspheres [10, 13], have relatively small finesse and a large FSR compared to larger cavities. The FSR is the periodicity in frequency domain measured between single-mode interference

frequencies of the cavities and the finesse is defined by the ratio of FSR over the cavity linewidth. For sensing, a small finesse is beneficial as it allows measurement of a larger portion of the frequency spectrum around the resonant frequency. Similarly, a small finesse when locking a laser's frequency increases the frequency range before drifting out of lock with the cavity. Nonetheless, micro-cavities provide a challenge to both sensing and locking the stability of a laser frequency. Without adding a greater level of complexity, an attempt to noticeably increase the sensing frequency range and linearity prohibits tight frequency resolution [14].

There are various methods for locking a diode laser using current modulation, single sideband or fringe locking, phase detection, and combinations of laser chains that reduce the linewidth of the laser [15]. The laser linewidth is dependent on the time over which it is being evaluated. In many texts this is defined as the full width at half maximum of the atomic transition and measured over the spectroscopic interaction time, a period of hundreds of microseconds [16, 17]. The laser linewidth is further affected by low frequency jitter and thermal effects that can be compensated for by locking to a feedback signal.

The PDH method has been most widely used with free space FP etalons for gravitational sensing [12, 18] or linewidth measurements [19], and for remote sensing using fiber FP cavities with significant cavity length [20, 21]. Similar to FM spectroscopy, the PDH method locks the laser to a cavity resonant frequency using a phase modulation to sample the phase of the cavity outside of resonance. The resonant frequencies of the cavity are defined by a mode number multiple of the FSR. A feedback signal is then received from the system that, when locked on resonance, is immune to laser amplitude noise fluctuations [5]. This signal is obtained by phase modulating the optical signal and homodyne mixing the output from the cavity infinite impulse response (IIR) filter as discussed in the section on PDH theory.

The devices used in the experiment are a mix of communications equipment and prototyped devices built for experimentation. The use of single-mode fiber for the signal connections mitigates noise that can be a significant factor in free-space optics with

multiple mode affects. Polarization control of the optical signal is important for matching incoming light polarization into the devices to maximize the transmission power and interference absorption to a single mode in the waveguides.

Either the laser or the cavity can be locked to the error signal. In many FP cavity locking setups, the error signal controls slight actuation of the laser or sensing cavity length to match the laser frequency with cavity resonance [22]. This allows the output from the cavity to be further locked giving a signal with very good stability. This has been recently accomplished for fiber systems using a fiber Bragg-grating that is tensile stressed [20, 21]. With micro-cavities, tensile acoustic modulation is more difficult and for this experiment the cavity will be thermally stabilized and mechanically isolated while the error signal provides feedback control to the laser.

2. OPTICAL FILTERING

Many of the techniques and math that are used to analyze digital filters are also used in optical filtering. Ring resonators and FP cavities have found uses in photonic signal processing as band-pass filters. As filters with low loss, these cavities can be used for sensing phase information. Much of the optical filter material found in this section and more has been thoroughly documented in references on optical filters [23]. The transfer function of a filter represents the output signal response to an input signal. Sampling this output signal allows us to use the math from discrete time systems.

In a single stage optical filter, the incoming signal amplitude is coupled into different optical paths. After traveling along the separate paths, these optical signals recombine and interference occurs between them. Interference occurs for signals that have the same polarity, the same frequency and are temporally coherent over the delay length. The waveguide over the short distance of transmission maintains this polarization. In these cavities the delay length is found from length of the cavity L and the propagation constant $\beta=2\pi f n_{eff}/c$. The delay length is equal to an integer multiple of βL, also represented in frequency space by the radial frequency Φ multiplied by the unit length T. The free spectral range is defined for optical cavities as in Equation 1.

$$FSR = \frac{c / n_{eff}}{(L_{round-trip})} \tag{1}$$

In this equation n_{eff} is the index of refraction of the waveguide and $L_{round\text{-}trip}$ is the effective length of the cavity. For a FP etalon, this will be 2*L and for a ring resonator it will be the ring circumference, π*D. More specifics of the cavities used in this experiment and how these values are found for them are covered in the section on optical devices.

The two types of cavities studied in this project are coherent infinite impulse response (IIR) filters. The response to an input is infinite in time and defined in frequency. There is at least one pole and one zero in the filter and these are coupled as will be shown. This type of filter can also be defined as an Autoregressive (AR) filter.

For a general discrete linear time system, the Z-transform is used to represent the response from an input signal. The Z-transforms have been widely developed for many optical filters to convert the discrete time signal into a representative frequency signal. The transfer function for this is shown in Equation 2. Note that optical filters can act on present and previous time signals only. There will be no response unless there is first an input to the cavity and thus these cavities are causal and the index of the transform summation begins at n=0.

$$H(z) = \sum_{n=0}^{\infty} h(n)\, z^{-n} \tag{2}$$

A discrete linear time input signal is represented in Equation 3. Finding the ratio of output to input of this signal results in the general Z-transfer function. This transfer function shown in Equation 4 is defined with the general coefficients *a* and *b*.

$$y(n) = b_0\, x(n) + b_1\, x(n-1) + \ldots + b_M\, x(n-M) - a_1\, y(n-1) - \ldots - a_N\, x(n-N) \tag{3}$$

$$H(z) = \frac{\sum_{m=0}^{M} b_m\, z^{-m}}{1 + \sum_{n=1}^{N} a_n\, z^{-n}} \tag{4}$$

Optical transforms have been defined for many frequently used cavities such as ring resonators and FP etalons. The approximation of the specific Z-transforms for a FP etalon and the ring resonator cavities used in this experiment is given in Equation 5. The general coefficients of Equation 4 can be determined from the FP and ring resonator coefficients in these transforms. The coefficients that are most often determined by experimentation are represented. [23]

$$H_{FP}(z) = \frac{-r_1 + r_2\, z^{-1}}{1 - r_1\, r_2\, z^{-1}} \quad and \quad H_{RR}(z) = \frac{\rho - \gamma\, z^{-1}}{1 - \rho\, \gamma\, z^{-1}} \tag{5}$$

Here r_1 and r_2 are the respective incident and back mirror reflection coefficients of the FP cavity. The variable ρ is the coupling coefficient between the ring resonator and the straight waveguide and the transmission coefficient is γ, where $(1-\gamma^2)$ is the percentage of power loss per cycle through the ring resonator. The z-transfer function coefficient z^{-1} is equal to exp^(j 2 π ω/ν), where ν is the cavity FSR. Note that the greater the value of γ, the less total loss there is in the ring. The optical cavities are shown in Figure 1 with the respective reflection, coupling, and transmission coefficients and optical paths shown.

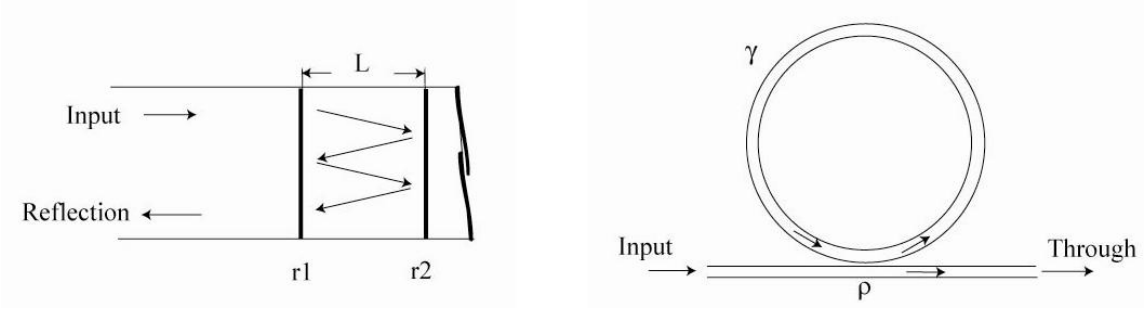

Figure 1 - FP and RR cavity optical paths

Optical Filter Response

For the ring resonator and FP cavity there is one pole and one zero for the transfer function as defined in Equation 5. A zero is the root of the numerator of the transfer function driving it to equal zero and the pole is the root of the denominator. Pole-zero diagrams are used as a qualitative approach to determining the characteristics of the filter.

Comparing the transfer function of a ring resonator with the Z-transform general form, the *a* and *b* coefficients can be found. These are shown in Table 1 and are the coefficients used to determine the magnitude, phase, and pole-zero plots.

Table 1 - Transfer function coefficients

	Ring Resonator	Fabry Perot Etalon
b0	ρ	-r1
b1	-γ	r2
a1	-ρ*γ	-r1*r2

The phase, magnitude, and pole-zero diagrams can be used to estimate the expected response of the cavity. The coefficients can be both real and imaginary to give a more precise model of the cavity response. The coefficients and transform equations can also be scaled using numerous rings and FP cavities to achieve a desired response. The pole-zero diagram has been shown to be useful for estimating the change in cavity response for single and multiple ring cavities in [24].

The phase and magnitude of an ideal ring resonator with loss is plotted in Matlab and shown in Figure 2. The phase response as seen in the first plot of Figure 2 has opposite sign polarity about resonance dependent on whether the input frequency is greater or less than the resonant frequency. The magnitude and phase are shown for the normalized frequency measurement offset between resonance and FSR. In this figure, the coupling and transmission coefficients are ρ=0.9 and γ=0.8.

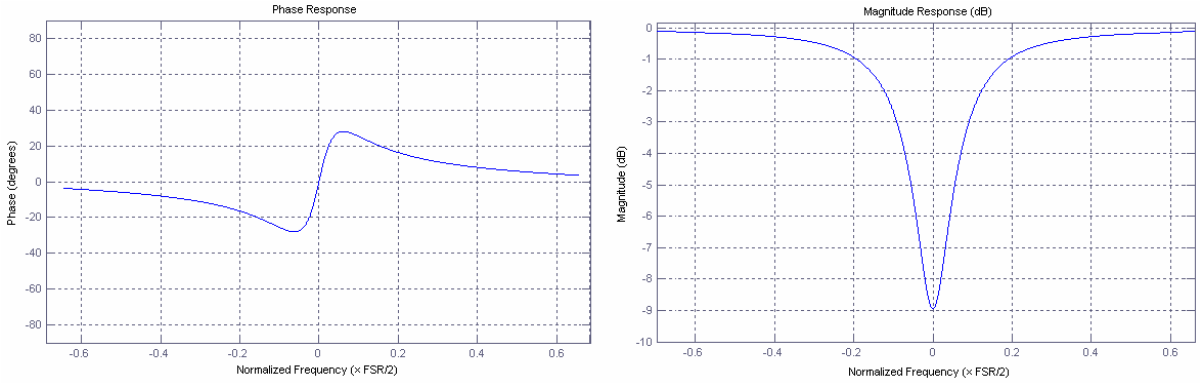

Figure 2 - Phase and magnitude response of a RR around resonance

The pole-zero diagram of this filter is shown in Figure 3 with a zero inside the unit circle, called a minimum-phase zero. The movement of the pole and zero along the real and imaginary axis changes the response of the filter. The zero will have greater magnitude than the pole for ring resonator filters unless considering an ideal all-pass filter with the cavity coefficients equal to one.

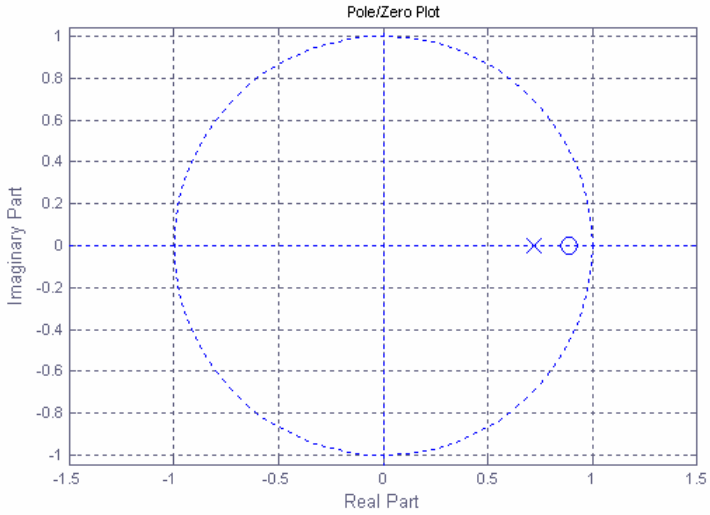

Figure 3- Ring resonator pole-zero diagram showing a minimum phase zero

The FP cavity in this experiment will differ in response from the ring resonator. Because the cavity back mirror reflection coefficient is greater than the front mirror reflection coefficient, the approximation of the phase does not return to zero between the resonant frequencies. This does not change the way we treat this filter compared to the ring resonator cavity, but it does increase the phase magnitude around resonance. The magnitude and phase of this cavity is simulated in Figure 4.

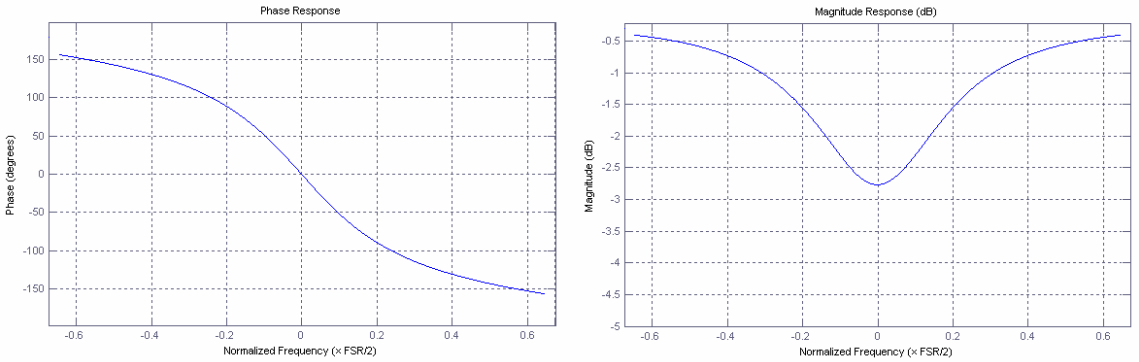

Figure 4- Phase and magnitude for an overcoupled FP cavity resultant from a maximum-phase zero design

The coefficients used here are, r_1=0.5 and r_2=0.9 to represent the prototyped FP cavity built for this experiment. This state where $r_2 > r_1$ is known as the overcoupled

state and the zero outside of the unit circle is considered a maximum-phase zero. The difference in the response of this type of filter can best be seen in the pole-zero diagram as shown in Figure 5.

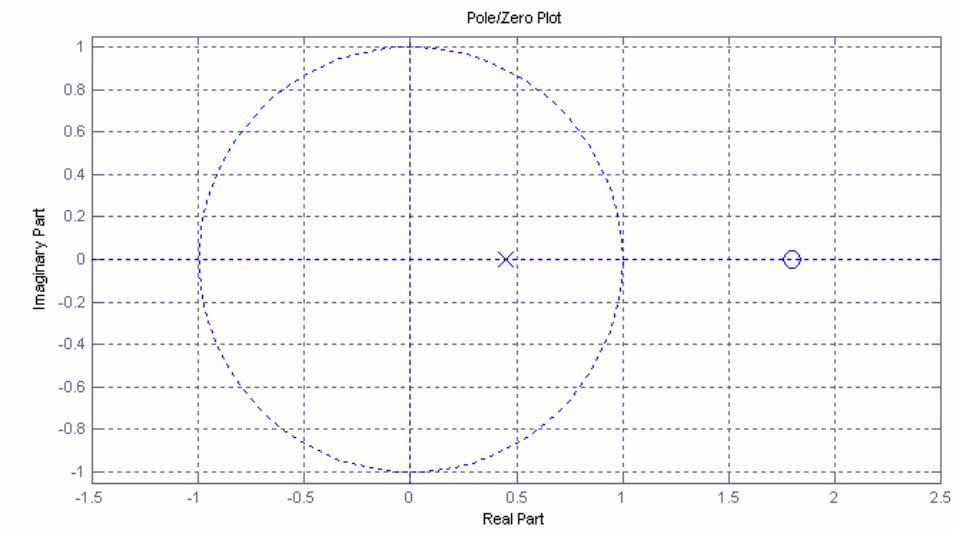

Figure 5- Pole-zero diagram for FP cavity with a maximum phase zero location

Because the phase shifts by 2π radians around resonance for this FP cavity, the slope of the phase at resonance is large, even though the reflection coefficient in this example is small. This example cavity has a larger phase transition range and amplitude than the minimum-phase zero cavity. Another factor to note is that the FSR of the FP cavity is much smaller than that of the ring and the phase transition is limited to a smaller frequency range.

The PDH method benefits from filters that have maximum-phase zeros because the slope of the phase around resonance is greatly increased. This slope increase is apparent in Figure 6 with the same coefficients interchanged to show the minimum and maximum-phase zeros. The magnitude response for these two filters is the same, but the slope of the phase is increased for a maximum-phase case when the transmission coefficient of a ring resonator γ, is greater than the coupling coefficient, ρ. Critical coupling occurs when these two coefficients are equal. This provides a high phase transition slope and also a diminution of light intensity at the resonant frequency.

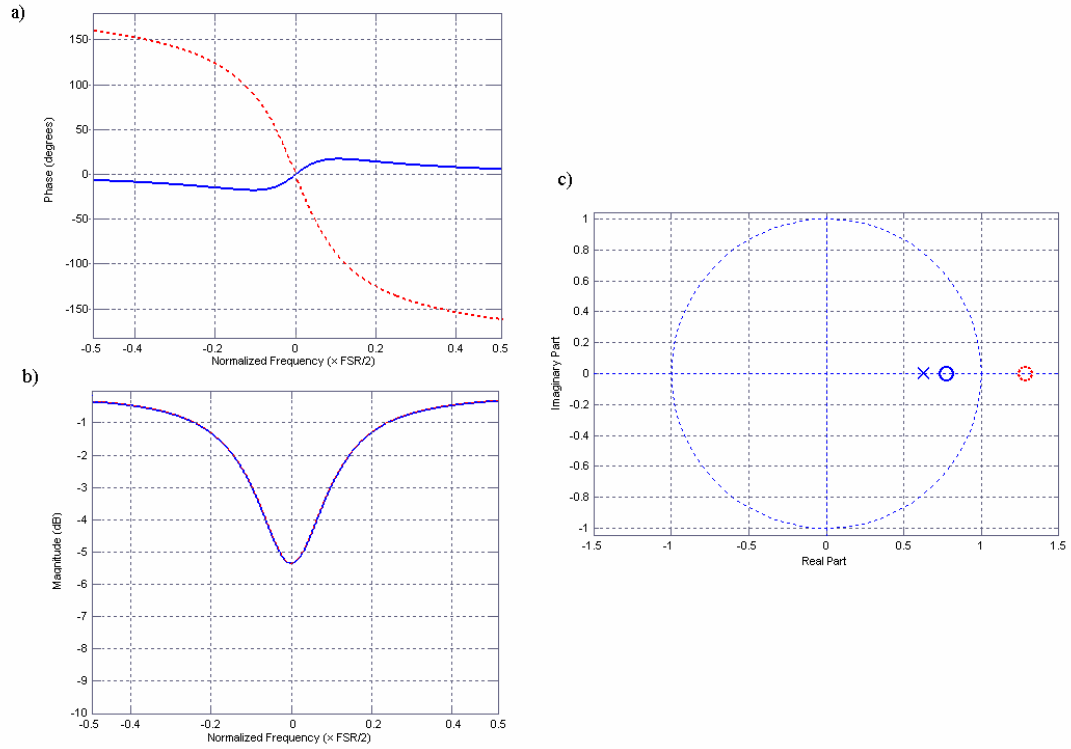

Figure 6 – A ring resonator with interchangeable values of 0.9 and 0.7 for coupler and transmission coefficients plotted for minimum and maximum phase zeros in a) phase b) magnitude and c) pole-zero plots

A filter with a maximum-phase zero will give the largest S/N of the phase transition for the PDH method as it crosses the resonant frequency and the greater offset from critical coupling will provide a greater slope. The phase slope seen for the maximum-phase zero in Figure 6 has the greatest slope immediately around resonance. The transmission can be further increased if gain is applied to the ring [25].

As seen, the phase can not be categorically determined from magnitude measurements. Group delay plots however can be shown to determine whether the response has minimum or maximum-phase zero. The group delay in Equation 6 is found by taking the derivative of the phase delay of the transfer function from [26, 27].

$$\tau = \frac{-\delta\phi}{\delta\omega} = \frac{-\delta}{\delta\omega}\left(\frac{\gamma(1-\rho^2)\,Sin\left(\frac{\omega}{FSR}\right)}{(1+\gamma^2)\,\rho - \gamma(1+\rho^2)\,Cos\left(\frac{\omega}{FSR}\right)}\right) \tag{6}$$

The group delay plot varies dependent on whether the zero is at minimum or maximum-phase for the cavity. This is seen in Figure 7 for various transmission variables from less-than to greater-than the coupling coefficient.

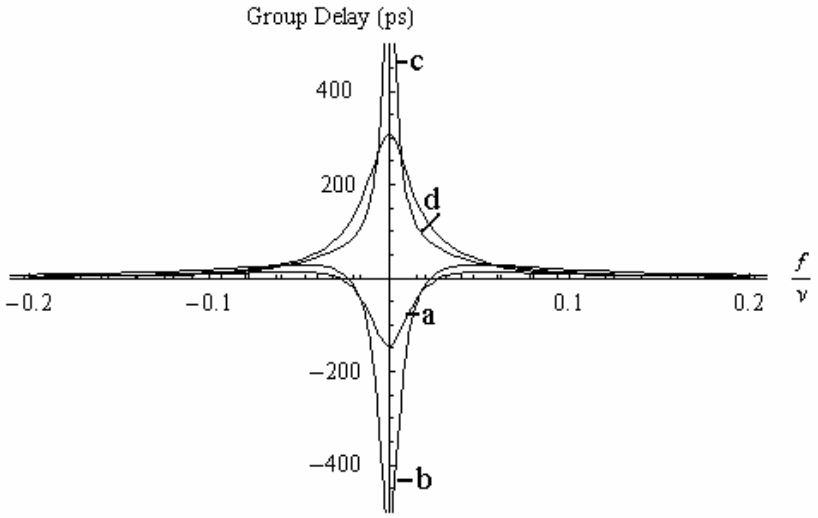

Figure 7- Group delay of ring cavity with ρ=0.875 and transmission coefficients equal to a) 0.8 b) 0.85 c) 0.9 d) 0.95

Group delay plots are taken for the devices in this experiment by a setup in the Photonics Signal Processing group at Texas A&M and will be discussed in the section on optical devices. We have seen how the phase and magnitude of the optical filters are related and discussed what this means for the PDH method. It is next shown how to apply the PDH method to sample the phase around resonance for these devices.

3. PDH PHASE MODULATION THEORY

The PDH method is similar to FM spectroscopy used for measuring biological samples. Both methods sample the phase of a laser signal response to one of a cavity's resonant frequencies. It will be shown how feedback from this method is an error signal that mitigates much of the laser amplitude noise when locked on resonance. This is accomplished by phase-modulating the optical signal and homodyne mixing the output from the cavity IIR filter to create the error signal [3, 5].

An optical signal can be represented simply as in Equation 7, which will be used for illustration of phase modulation. The phase modulation is encoded in the plane-wave oscillating signal in addition to the frequency dependence.

$$Signal = A\,Cos\left(\omega t + \phi shift(t)\right) \tag{7}$$

The phase shift variable, $\varphi shift$ can be fixed or dependent on time as considered here. There is also intrinsic phase information of the laser that is unknown and is a constant that we subtlety add to the frequency 'ω'.

In the frequency spectrum, a set phase addition to the signal will shift the frequency of the signal by that phase amount. A time varying phase addition in the form of a sine function will allow multiple frequencies offset from the signal center frequency at positive and negative multiples of the modulation frequency. This time-variance phase modulation is shown to induce a center carrier frequency and first order side bands as in Figure 8 using a coherent optical spectrum analyzer.

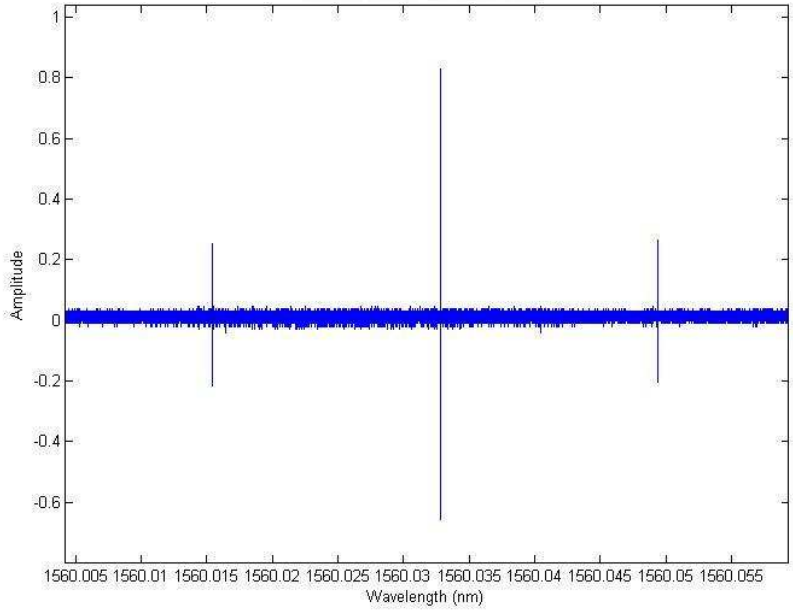

Figure 8 - Carrier and sidebands in frequency domain with 1.9GHz phase modulation taken from a coherent optical spectrum analyzer (COSA) setup

The bandwidth of the signal after modulation is given by Carson's rule in Equation 8. This describes the width in frequency-space of the signal and incorporates the significance of the sidebands in the frequency domain. The bandwidth determines how much of the frequency spectrum is used to encode this signal without interfering with frequencies outside of this range. Multiple signals are able to be encoded within this range or outside of it, but to mitigate noise in this experiment, a single modulation signal is used.

$$BW = 2(1+\beta)\varphi \tag{8}$$

In the equation β is the modulation index and φ is the modulation frequency. The modulation index determines how much power is distributed between the carrier and the sidebands. A greater modulation index will take up a larger bandwidth as further order sidebands appear. These sidebands are a result of the harmonics of the phase modulation

and further sidebands appear at multiples of the modulation frequency offset from the carrier frequency.

A traveling wave from the laser with a single frequency is assumed for the PDH calculation input into the phase modulator. The electromagnetic wave at the output of the phase modulator is then represented by the signal in Equation 9.

$$E_{\text{mod}} = E_0 \, e^{j(\omega t + \beta \sin(\phi t))} \tag{9}$$

In this equation $\beta \sin(\varphi t)$ represents the modulation signal, and φ is the modulation angular frequency.

The Jacobi-Anger expansion is applied to this function to represent it as a sum of Bessel functions [28]. The modulation depth will limit the power to the carrier and first order sidebands so the equation can be further approximated with 0 and 1rst order Bessel functions as shown in Equation 10.

$$E_{\text{mod}} = E_0 \, [J_0(\beta) \, e^{j\omega t} + J_1(\beta) \, e^{j(\omega+\phi)t} - J_1(\beta) \, e^{j(\omega-\phi)t} + \ldots] \tag{10}$$

Here it is more apparent that the phase modulation has created a center carrier wave input into the modulator and two sidebands offset by the modulation frequency; one at positive φ and the other at negative φ. The amplitudes of the sidebands depend on the modulation index and will be smaller than the carrier signal. In order to choose a modulation depth dominated by the carrier and first order sidebands we want further order sidebands to be small. The graph of the first three orders of Bessel functions is shown in Figure 9.

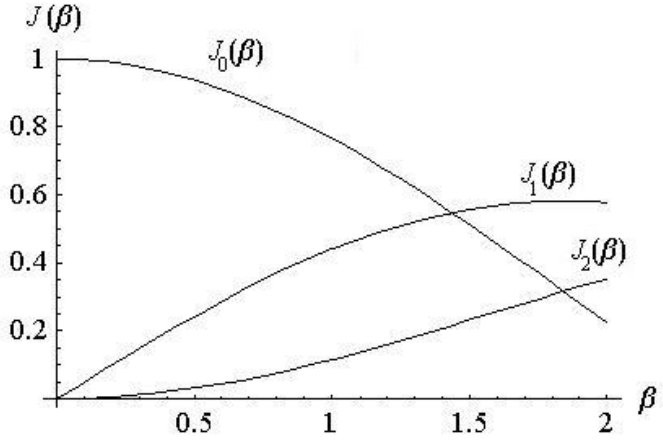

Figure 9 - Bessel functions graph

The modulation index β, is able to be found from the averaged measurement of output magnitudes of the carrier and sideband signals. The average ratio of carrier to first order sideband is detected in experimentation and matched to the graph. First order sidebands are used because noise is added and the carrier signal has less power with further orders of sidebands. Because the PDH method uses sampling of the phase of the two first-order sidebands with the carrier, any further orders of sidebands do not add to the error signal. The modulation index can be increased by adding power to the modulation signal.

The modulation index will be kept at less than one so that the carrier signal is significantly larger than the sideband signals while further sidebands of larger ordered Bessel functions are kept minimal. The optimum depth of 0.83 is found by adding twice the first-order Bessel function to the zero-order function and subtracting greater orders. The product of this method is relatively flat around the optimum index, so values can be offset from the optimum depth and not significantly affect the experiment.

The optical signal from the phase modulator is input to the cavity to be used for locking or sensing. The specific transfer functions for the cavities are discussed in the optical filters section. The math maintains its similarity for the Fabry-Perot and ring resonator cavities used in this experiment to determine the feedback error signal.

The transfer function of the cavity is multiplied by the incoming electric field to give the signal response of the mixing between the phase interactions. The transmission of the electric field through the Fabry-Perot cavity is defined in Equation 11 for the PDH method [5].

$$E_{transmit} = E_0 [J_0(\beta) e^{j\omega t} H(\omega) + J_1(\beta) e^{j(\omega+\varphi)t} H(\omega+\varphi) - J_1(\beta) e^{j(\omega-\varphi)t} H(\omega-\varphi)] \quad (11)$$

In this equation H(ω) is the transfer function of the cavity while H(ω ± φ) is the response at the sidebands and will be represented from here on as H_+ and H_-.

The intensity signal is shown in Equation 12 to start the progression of this method to a form able to be homodyne mixed to an error signal. The Bessel functions and power amplitude coefficients are pulled out of the cavity response signal so the focus can be on the variables and determinants that define the response.

$$P_{transmit} = P_0 [|H|^2 J_0^2 + |H_-|^2 J_1^2 + |H_+|^2 J_1^2 + J_0 J_1 e^{-j\varphi t}(H H_+^* - H^* H_-) + J_0 J_1 e^{j\varphi t}(H^* H_+ - H H_-^*) + 2\varphi terms] \quad (12)$$

The terms that will be homodyne mixed to DC have dependence on the first order of the modulation frequency, not its harmonics. These are shown in the second line of Equation 12. We will continue to use these values and the rest of the power will be filtered out at the mixer and low-pass filter. Using Euler's identity to separate the exponents will be helpful later and the result is shown in Equation 13. The Cosine and Sine terms are separated- note that the real and imaginary terms are not exactly the same, but can be reduced to twice the $H^* H_+ - H H_-^*$ set for both cases.

$$\begin{aligned} P_{transmit} &= P_0 J_0 J_1 \{\mathrm{Re}[H H_+^* - H^* H_- + H^* H_+ - H H_-^*] Cos[\varphi t] \\ &\quad + \mathrm{Im}[H^* H_- - H H_+^* + H^* H_+ - H H_-^*] Sin[\varphi t]\} \\ &= 2 P_0 J_0 J_1 \{\mathrm{Re}[H^* H_+ - H H_-^*] Cos[\varphi t] \\ &\quad + \mathrm{Im}[H^* H_+ - H H_-^*] Sin[\varphi t]\} \end{aligned} \tag{13}$$

The RF signal from the detector is input into a high frequency mixer with the local oscillator (LO) signal from the signal generator. The input frequency of the LO signal, θ is equal to the RF frequency used in the optical phase modulation, φ. The output produces a signal at DC for either the real or imaginary terms that will be used in the error signal. This is dependent on the phase of the LO signal input to the mixer compared to the RF signal from Equation 13.

The trigonometric identities for mixing two waves are given in Equation 14. The two states that provide the largest DC output are when the signals are matched for input into the mixer using either cosine or sine. The signal into the LO port is from the RF generator and has a phase shift added to match the desired input signal from the detector. The signals have matched phase for the real part of the error signal response and are in quadrature for the imaginary part of the error signal response. A phase difference between these two states reduces the DC component of the error signal around resonance.

$$\begin{aligned} Sin(\varphi) Cos(\theta) &= \frac{1}{2} Sin(\varphi + \theta) + Sin(\varphi - \theta) \\ Cos(\varphi) Cos(\theta) &= \frac{1}{2} Cos(\varphi + \theta) + Cos(\varphi - \theta) \\ Sin(\varphi) Sin(\theta) &= \frac{1}{2} Cos(\varphi - \theta) - Cos(\varphi + \theta) \end{aligned} \tag{14}$$

The amplitude coefficient of the phase matched and quadrature error signals are shown in Equation 15 after homodyne mixing.

$$\begin{aligned} &Matched \quad Error\ Signal: P_0 J_0 J_1 \,\mathrm{Re}[H^* H_+ - H H_-^*] \\ &Quadrature \quad Error\ Signal: P_0 J_0 J_1 \,\mathrm{Im}[H^* H_+ - H H_-^*] \end{aligned} \tag{15}$$

On resonance the error signal will be zero from the laser and transmission is at a minimum as seen in Figure 10. This signal is then immune to power amplitude noise from the laser that is independent of frequency shift. This is one advantage of the PDH method over other methods. The optimization of the error signal and the linear response immediately around the resonant frequency are further discussed in the section on slope optimization.

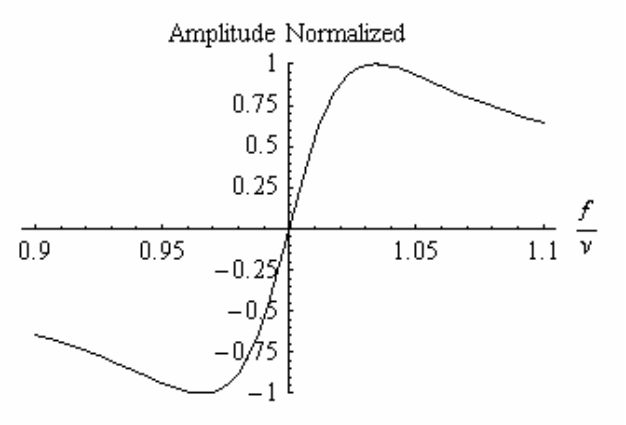

Figure 10 –Example of the DC error signal output at resonance versus the ratio of frequency to FSR

The PDH method is not bandwidth limited by the cavity. Incident light is stored in the cavity for the period of transition or one over the free spectral range. Any change of phase of either light in the cavity or incoming light creates a phase change and a difference in the error signal. Because of this, the signal feedback is not delayed by the length of the cavity if the sidebands are not resonant in the cavity. Any bandwidth limit is dependent on the delay of the feedback and receiver electronics [12].

The error signal from the phase response of a cavity changes due to intrinsic properties of the cavity such as linewidth and the free spectral range, and also extrinsic factors such as the method used to sample the phase. In the PDH method, the most

important variables able to be user-defined are the modulation depth and modulation frequency. For a cavity that is locking the laser, it is important that the error slope around the resonant frequency be as large as possible to get the greatest frequency resolution out of the signal. The quadrature-phase error signal slope around resonance increases for any modulation frequency greater than zero up to 50 percent of the free spectral range. The frequency range of the error signal is defined as the region of transition with a roughly linear slope around resonance. This range also increases as the modulation frequency increases to an extent discussed in the section on optimization.

To review, the PDH method is capable of sampling the phase around the resonance of an optical cavity. It has been shown to be capable of mitigating laser amplitude noise when locked on the resonant frequency. This is accomplished by phase-modulating the optical signal and homodyne mixing the output from the cavity IIR filter to create an error signal. The error signal has opposite sign polarity on either side of resonance allowing information on the resonant frequency. Feedback electronics can then be used to lock this signal.

4. OPTICAL DEVICES

The axiom has been stated that to get a good response from the PDH method, the modulation frequency must be very much greater than the cavity linewidth [12, 19, 20, 21]. This does not take into account cavities with low finesse or small cavities. This also does not address the maximum limit of the modulation frequency affect on the error slope, which is more difficult to obtain on smaller cavities but easily reached when testing large FP cavities.

The range of frequencies absorbed by the filter is determined by the finesse of the cavity as shown in Equation 16. Here the FP etalon reflectivity coefficient, R is the reflection coefficient of two identical mirrors without loss. The ring resonator coefficients ρ and γ have a similar response on the cavity and their product can be substituted into Equation 16 for R. [25, 29].

$$F \cong \frac{\pi\sqrt{R}}{1-R} \tag{16}$$

The finesse is not a direct measurement from the cavity magnitude response. Instead, an approximation is found from the linewidth and free spectral range of the cavity. The free spectral range is the measurement between single-mode interference valleys of the cavities. The linewidth is approximated from the full width across the resonant frequency at half maximum. Finesse is found from the ratio shown in Equation 17. From this equation, further coefficients of the cavity can be determined to find the optimum modulation frequency and define the expected response of the cavity.

$$LW = \frac{FSR}{Finesse} \tag{17}$$

The high value for the finesse and the quality factor of the ring resonator are important in this experiment. A higher Q-factor affects the width of the resonant valley allowing more off-resonance frequencies to be transmitted. This represents a smaller linewidth value for the valleys as found in the Equation 18.

$$2Q_c = 2\left(\frac{\nu_0}{\Delta\nu_{\frac{1}{2}}}\right) \tag{18}$$

In this equation, ν_0 is the resonant frequency and $\Delta\nu$ is the -3dB linewidth. The Q-factor is a measurement for the frequency comparison to linewidth similar to the finesse measurement of the periodicity in the frequency domain compared to the linewidth. The reflectivity or transmission coefficients for ring resonators and FP cavities are close to one in high-Q cavities. This decreases the linewidth compared to the FSR and increases the slope of the PDH error signal.

Energy is able to be stored in the cavity over a short period of time. The amount of power that can be stored and built up in the cavity using the PDH method is found from the circulating power multiplied by one over the free spectral range in Equation 19 [16].

$$P_{stored} = P_{in}\, J_0^2(\beta)\frac{Finesse}{\pi\, FSR} \tag{19}$$

The light is delayed by the distance it must travel around the loop of a ring resonator or twice the cavity length of a FP etalon. The power in the cavity is proportional to this light delay. Further, the drop-port from a ring resonator or the leakage beam from an FP cavity can act as a stable average of the cavity and input frequency [3].

Cavity PDH Error Signal

The theoretical plots of the error signals in Figure 11 show the increase in error slope and S/N ratio for a FP etalon as the modulation frequency increases as compared to the free spectral range. This cavity has a fairly low finesse of 30 to compare it with ring resonators.

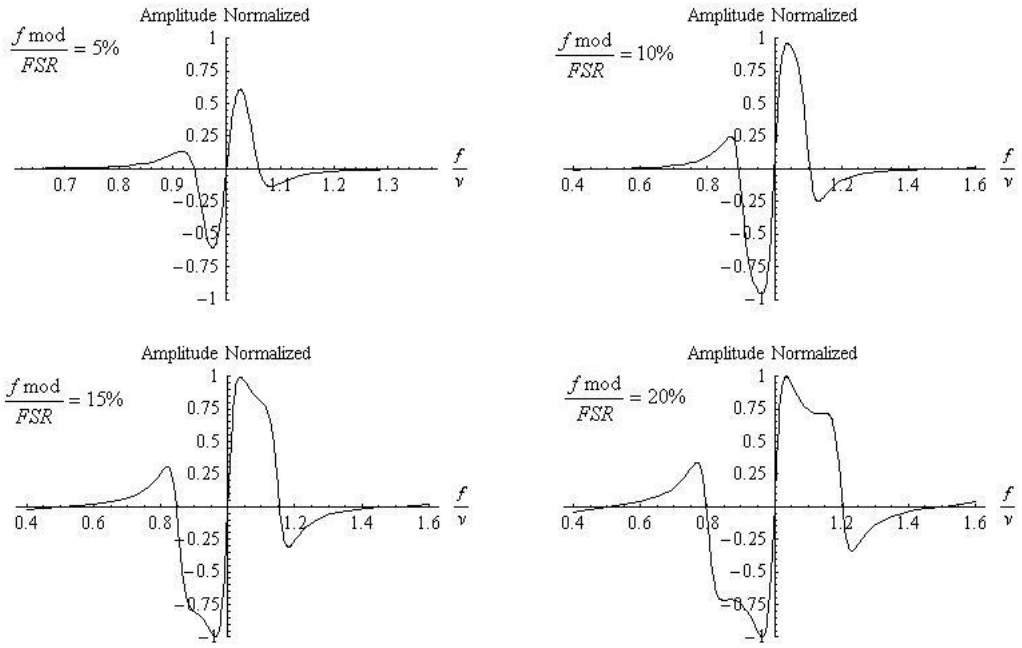

Figure 11- FP error signal graphs for modulation frequency of 5, 10, 15 and 20 percent of FSR with reflection coefficients equal to 0.9

The error signal for the ring resonator has similar shape and response around resonance compared to the FP cavity. The frequency response allows the same linewidth behavior between the two types of cavities differing predominately in the magnitude of the FSR. The graphs in Figure 12 show a greater total increase in error slope and S/N ratio than found in the FP cavity as the modulation frequency increases. There is also a much more significant frequency difference between the two plots as ten percent of the FSR of a fiber FP cavity can be in the MHz range and for the integrated ring resonator is tens of GHz. An increase in the error signal frequency range for the ring resonator as the modulation frequency increases is also apparent.

In this case, twenty percent of the FSR for these graphs results in a slope approaching the maximum slope while the frequency range only changes little and is similar to the lower modulation frequency. In these graphs, the cavity response is shown to have a dependence on the modulation frequency that can be optimized.

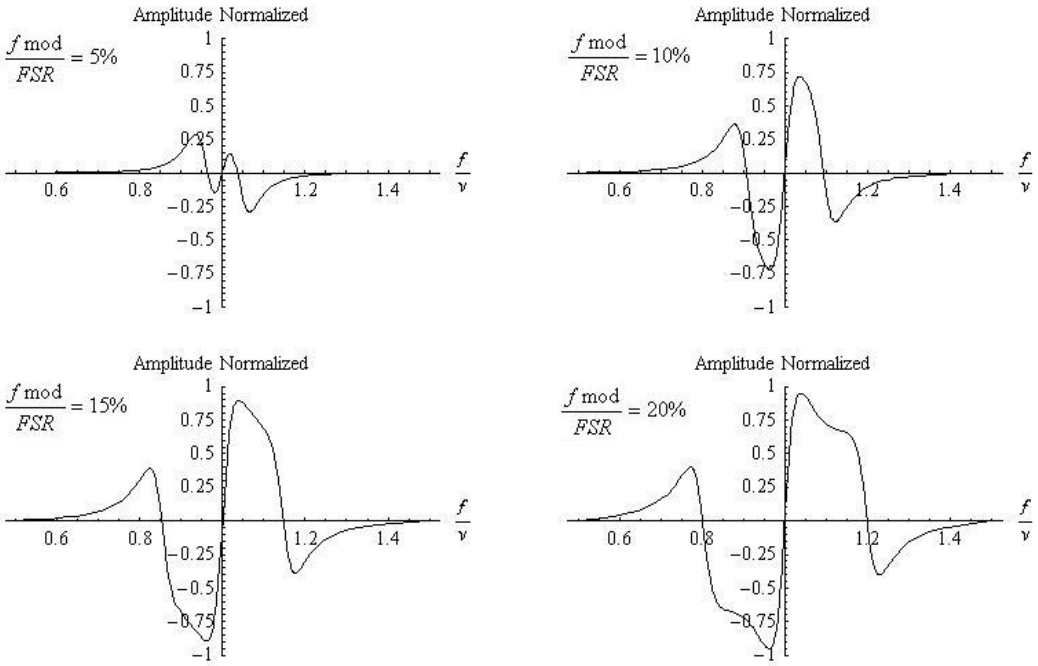

Figure 12- RR error signal for modulation frequency of 5, 10, 15 and 20 percent of FSR in a lossless case with coupling coefficient equal to 0.8

Fiber Fabry-Perot Cavity

The transmission through a FP etalon can be used as a pass-band filter and for filtering optical frequencies. Conversely, the reflection is an IIR filter allowing destructive interference of frequencies that are narrowly within range of a resonant frequency of the cavity.

The transfer function of the reflection as shown in Equation 20 is dependent on the amplitude reflection coefficient, the input frequency of the laser, and the free spectral range defined by the device.

$$H(\omega) = \frac{R(e^{j\frac{\omega}{\nu}} - 1)}{1 - R^2\, e^{j\frac{\omega}{\nu}}} \tag{20}$$

In the equation, the variable R is the reflection coefficient, ν is the FSR frequency and ω is the laser angular frequency.

In the case where the FP cavity has a reflectivity of 100%, allowing R=1 and no loss, the reflected signal would see the cavity as a true all-pass filter and there would be no resonant interference frequencies. However, FP cavities have a reflectivity of less than one, allowing for energy to be accumulated between the mirrors on resonance. The range of frequencies resonant in the filter is determined by the finesse of the FP cavity.

Higher finesse cavities are available for FP etalons than for integrated ring resonators both because the etalons are larger and the design limitations of ring resonators. Integrated and fiber FP cavities are also limited by design and fabrication techniques of reflective surfaces. Intrinsic FP cavities have these reflective surfaces part of the guiding medium compared to extrinsic cavities that reflect off of surfaces between the guiding medium and free space.

An intrinsic fiber FP cavity is designed in this experiment for intermediate locking of the laser. The advantage of a fiber FP cavity is its smaller FSR value, which has a resonant frequency every 4GHz instead of hundreds of gigahertz as for the ring resonators. The cavity has been created by splicing a titanium oxide coated-end fiber to a single-mode fiber. The far end of this fiber is then cleaved and a gold coating is sputtered onto the end to induce a very high reflectance of the back mirror.

Since the reflectivity is relatively low resulting in low finesse, the linewidth of the cavity will be large. Increasing the reflectivity allows a larger finesse, reducing linewidth and allowing sidebands to be outside of resonance. In this case, the sidebands are promptly reflected off of the incident mirror and give good sampling of the phase of the carrier frequency compared to cavity resonance.

Ring Resonators

A through-port ring resonator transfer function responds similar to the reflection signal from a FP etalon. Instead of storing energy in a cavity between two mirrors, it stores energy in a small ring waveguide that couples to a transmission waveguide running tangential to the ring. The transmission transfer function of the ring resonator is

shown again in Equation 21. This is the function used in the power transmission through the cavity of Equation 11.

$$H(z) = \frac{\rho - \gamma\, e^{-j\Phi}\, z^{-1}}{1 - \rho\, \gamma\, e^{-j\,\Phi}\, z^{-1}} \tag{21}$$

Variables are in a refined form to simplify the equation. Here ρ is the coupler coefficient for the throughput power, $(1-\gamma^2)$ is the cavity loss and Φ is the phase shift of the pole. The z-transfer function coefficient z^{-1} is equal to exp(j 2 π ω/FSR) [23].

Because the device is small, the FSR of a ring resonator is on the order of hundreds of GHz. The ratio of the modulation frequency and laser frequency to FSR will be important in determining the phase of the laser as it resonates in the cavity. With the high finesse of the Sandia and Nomadics ring resonators, frequency sensing with a high S/N ratio is obtainable.

Sandia Ring Resonator

A ring resonator has been loaned to this project from Sandia National Labs. The paper from the Sandia researchers outlines the construction and some characteristics of the resonator cavity [30]. The ring resonator is made from a silicon nitride deposition and etching of a waveguide onto a silicon-oxide chip. The index of refraction of the silicon nitride is 1.98, higher than the silicon oxide and allows the light to be internally refracted.

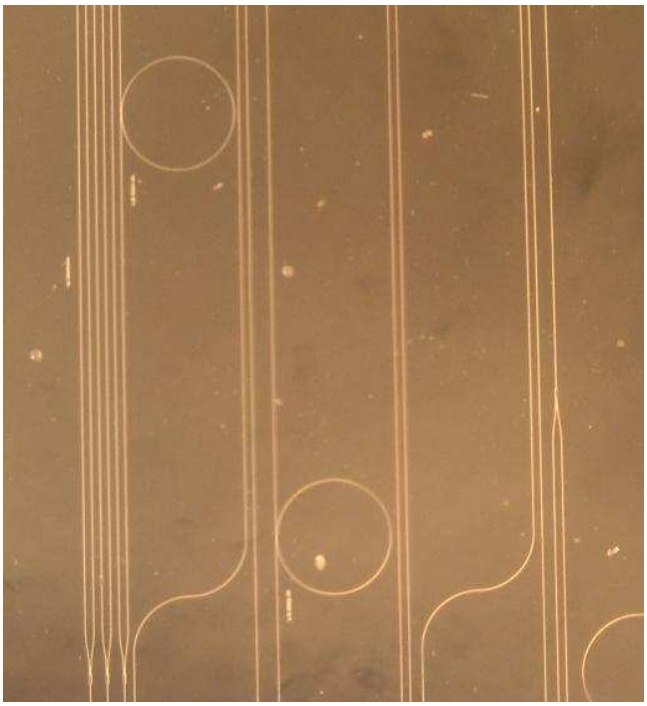

Figure 13 - Sandia RR in waveguide showing transmission and coupled ring waveguides- the ring diameter is 680µm

Optical fiber is connected to each side of the chip with lens coupling to collimate the signal and allow the signal to pass into the waveguide. The waveguide and the lower coupled ring shown in Figure 13 are used in this experiment. The characteristics of the ring resonator are determined by a laser sweep across the frequency spectrum under concern for this experiment. This is the region from 1559-1561nm and is shown in Figure 14.

A Q-factor of 2.4×10^5 is determined for this ring resonator. The ring is 680 micrometers in diameter resulting in a FSR of about 140GHz. The device has a total loss on the order of -19dB from the lens coupling. This is a significant loss and care must be taken to receive meaningful output from the ring cavity.

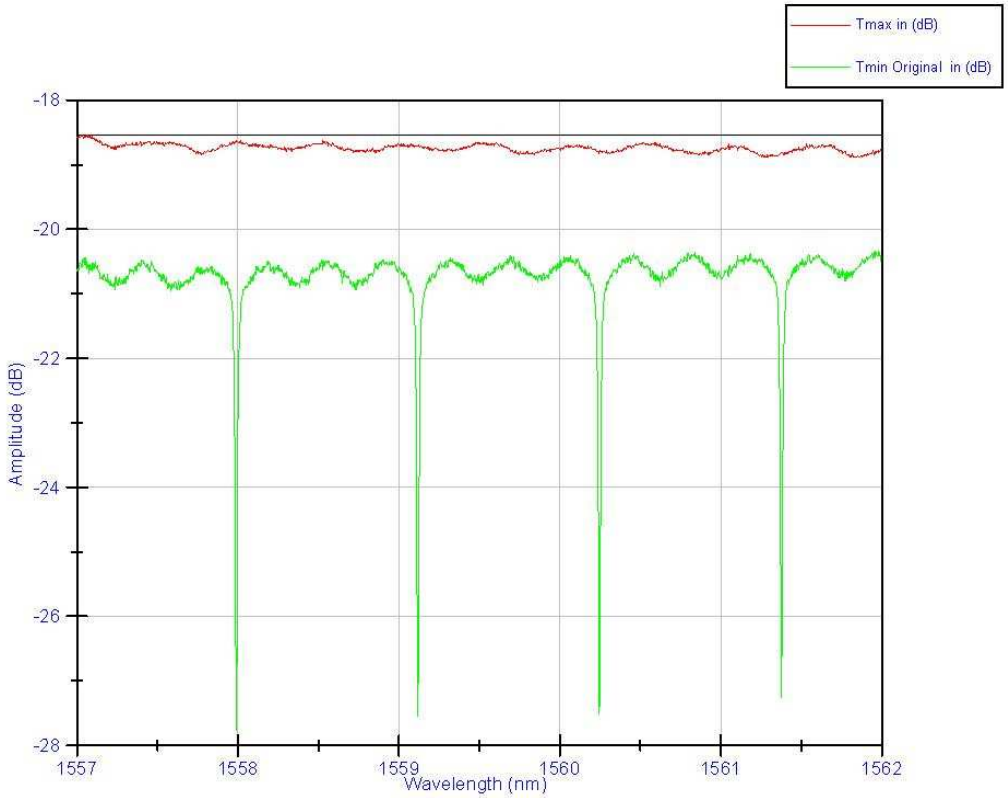

Figure 14 – Sandia RR polarization max and minimum transmittance

The laser input power to the ring resonator is less than two milliwatts. Therefore, the transmitted signal from the ring resonator must be amplified in order to have a signal capable of being detected. An erbium-doped fiber amplifier is added after the ring resonator to amplify the signal.

The ring is covered by a thin layer of silicon oxide and environment factors shift the resonant frequency of the ring resonator. The change in the index of refraction due to a change in environment or temperature or strain can be analyzed to determine what material is causing the shift and lead to further research material. This will be discussed later in the conclusion and future works sections.

Nomadics Little Optics Ring Resonator

Another ring resonator loaned to the photonics group at A&M is from Nomadic's Little Optics Division. It is an integrated ring resonator with a through and drop port.

The through-port provides the response used for the PDH error signal. The magnitude response is shown in Figure 15 for maximum and minimum transmission polarization states. It can be seen in the figure that this ring has little amplitude destructive interference on resonance, proving difficult to obtain an amplitude dependent discrimination of frequency at resonance.

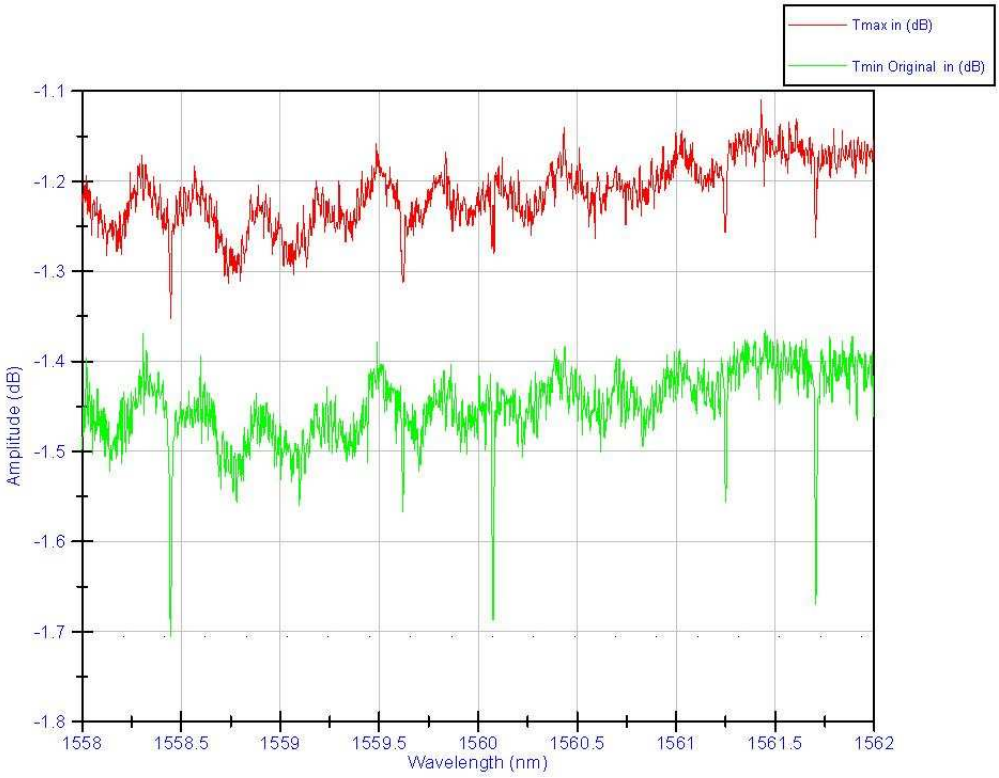

Figure 15 - Nomadics RR through-port polarization max and minimum transmittance

Group Delay

Characteristics of the cavities in this experiment have been detected using the group delay measurement setup at Texas A&M [31]. The group delay of the Sandia and Nomadics ring resonators at their respective resonant wavelengths is shown in Figure 16. The phase changes at resonance because the light coupled into the cavity is delayed for a period of time and will lead or lag the phase of the light propagating through the waveguide separated by a coupler shift of $\pi/2$. The group delay is the derivative of the phase delay of the cavity.

These cavities can be seen in Figure 16 to have different phase-zero responses. The Sandia has negative group delay offset while the Nomadics has positive group delay at resonance compared to the group delay immediately around resonance. From this, it is determined that the Sandia ring will have a minimum phase-zero response and the Nomadics will have a maximum phase-zero response.

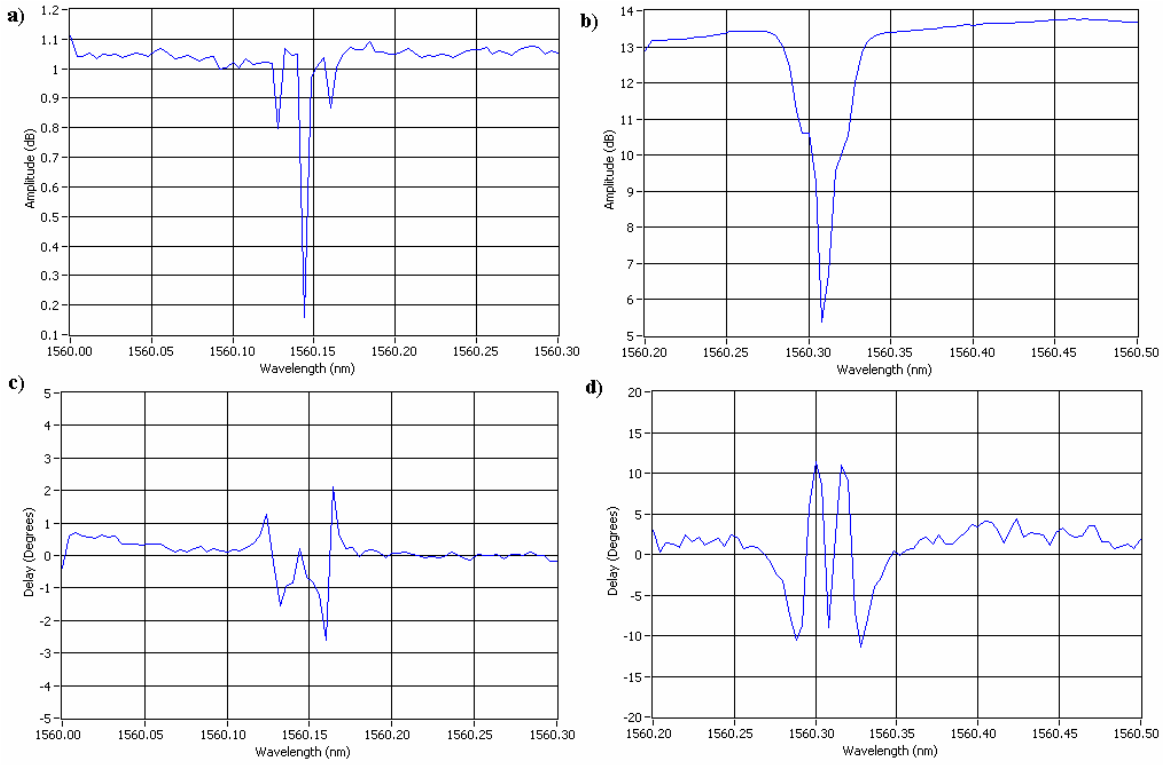

Figure 16 - Ring resonator cavity plots for magnitude of the a) Nomadics ring and b) Sandia ring with optical amplification. The group delay plot is in c) for the Nomadics and d) for the Sandia ring

Laser and Optical Amplification

The laser chosen is very important for many locking experiments. In many applications, a small linewidth and low drift is important. For this experiment to demonstrate a high frequency modulation lock, the laser is a less critical component. It must be able to sweep the spectrum around resonance with capable input resolution tight enough to lock onto the cavity. The laser must be locked so that detection by the cavity is not altered by the outside environment of the laser and the locking system.

Two lasers are used in this experiment; the predominant one is a commercial distributed feedback (DFB) package D2526 with fiber output from Lucent. This type of laser is a fairly inexpensive component used in optical communication systems and similar lasers been used in previous locking techniques [32]. The ability to lock and sense with this laser will continue to lay the foundation for future commercial possibilities. A second laser from Orbits Electronics with a piezoelectric transducer control of the laser cavity is tested. This laser has a much lower frequency tuning range and a much smaller linewidth resulting in less noise in the error signal as discussed in the results section.

The DFB laser has two inputs to control frequency. A built-in thermo-electric controller monitors the temperature of the laser chassis and a laser diode controller (LDC) limits the drive current with modulation input available. The temperature controller can be adjusted with control steps of ten of ohms. The temperature resistance is held within 1 ohm as the current is controlled around resonance. The temperature does not vary outside of the specified resolution for small changes in current input.

The current has been chosen as the user defined control of the laser because a change in drive current has a much quicker settling time than a change in temperature. The laser has a maximum laser diode current of 150mA to sweep across the 1558-1564nm range, though the full range will not be used.

The output current to drive the laser is controlled via an input voltage to the LDC. A negative voltage input will lower the output current and a positive voltage will raise the current and the LDC follows a linear ratio to vary 0.0122mA laser current for every 1mV minimum input step to the laser diode controller. It has been tested that a 1mA step varies the laser by 0.0039nm. Therefore the input of 1mV increases the wavelength by 0.048±0.02pm.

The frequency variation can be less for a further stabilized DC source. However the source used from the computer has a minimum output resolution ± 0.5mV and the resultant frequency control resolution is less than what the PDH system is capable of

discriminating. The conversion from a variance in wavelength to frequency at the resonant frequency is shown in Equation 22 for clarity.

$$\Delta frequency(\delta\lambda) = \frac{c/n_{eff}}{1560.2*10^{-9}} - \frac{c/n_{eff}}{1560.2*10^{-9} + \delta\lambda} \tag{22}$$

The laser linewidth from the manufacturer is stated to be 2-10MHz. The laser in this experiment is estimated to be 10MHz from delayed self-heterodyne interferometry [33, 34, 35]. A coherent optical spectrum analyzer with a narrow-beam swept laser is also used to estimate the sideband offset of the modulated signal with a side benefit of estimating the beat note between the two lasers. The linewidth of the sweep laser is 6MHz ±1MHz. If the laser has a linewidth less than the sweep laser linewidth, then around resonance there will be a clear beat note of frequency less than the noise frequency of the signal around resonance. Because the beat note cannot be fully separated from the noise using the DFB laser, it is estimated that the linewidth is larger than 6MHz.

The laser will need to be locked on the order of its linewidth of 10 MHz to minimize interference with the limit resolution of the error signal measurements. This resolution has been previously demonstrated locked to gas absorption lines [30]. The limiting factor in this experiment is the linewidth of the laser. The DFB laser has each of its variables outlined in this section controlled so that the limit resolution measurement of the ring resonator is dependent on the linewidth of the laser around the resonant frequency.

The Orbits laser is used to make measurements at a more sensitive resolution due to a lower laser linewidth. The linewidth measurement of this laser is limited by the minimum noise in the cavity as the error signal feedback limiting resolution is an estimated 900kHz. Any laser linewidth less than this value will need to be further measured by an increased sensitivity. This laser is used to compare locking performance data of a more sensitive laser compared to the DFB diode laser. Due to its small frequency tuning range, the Orbits laser is not used for sensing both ring cavities.

It is found that the DFB laser has a feedback slope (mV/pm) closer to the error slope of the cavity than the Orbits laser, which has a much higher feedback slope. The feedback slope of the Orbits laser is 2.5V to tune the laser wavelength 1pm. The DFB laser tunes 1pm with 20.8mV meaning that there is a greater voltage output needed to the Orbits laser for a lock. Therefore, it is necessary to have greater gain added to the error signal feedback so it has a proportional affect on the control of the Orbits laser.

The erbium-doped fiber amplifier (EDFA) amplifies signals from 1520-1580nm with up to 20dB of gain. The gain added to this setup is typically 15dB. This increases the intensity of the entire frequency spectrum around cavity resonance by 15dB so transmission through an FP filter is used to filter out unwanted amplified spontaneous emission. The EDFA is connected after the optical cavity to limit the noise and power input into the cavity to the laser signal.

The Sandia ring and the FP cavity include the EDFA as part of the setup to increase the output power from the cavity to the detector. This is used because coupling to the devices involves unavoidable loss without better fabrication of the cavities. Optical amplification also has the benefit of increasing the slope around resonance.

5. EXPERIMENTAL SETUP

Locking the laser to a single cavity is accomplished with the Nomadics high-Q ring resonator. The setup for the experiment is shown in Figure 17. The cavity is in a thermally stable enclosure on the optical table. The detector is capable of measuring 10GS/s and the RF devices have sufficient bandwidth for the low GHz frequencies.

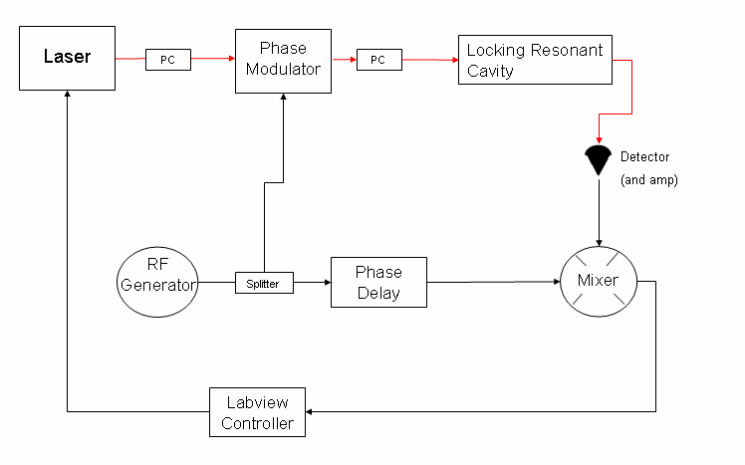

Figure 17 - Single cavity locking setup shown with the PID feedback that can be replaced with direct feedback

Environmental Test

Resonant frequencies for both the high and low-Q cavities are probed using the same signal output from the modulator. The cavity's resonant frequencies are held in a thermally stable state. With its greater finesse, the Nomadics cavity has its resonant frequency held within the error signal range of the Sandia cavity so that the laser frequency will be locked within a fraction of the cavity's total frequency range. The error signal from the ring resonator cavity with a stabilized laser is then utilized for temperature and environmental sensing.

What carry-over laser frequency noise there is from the locked cavity should be less than the resolution that can be measured using the sensor cavity. Since the Sandia ring cavity has a smaller finesse than the locking cavity, the error slope allows more frequencies to be sensed in the region of resonance in this cavity. This also allows

holding the laser lock over a long period of time within a small range of frequencies. This setup is seen in Figure 18 for the two cavities.

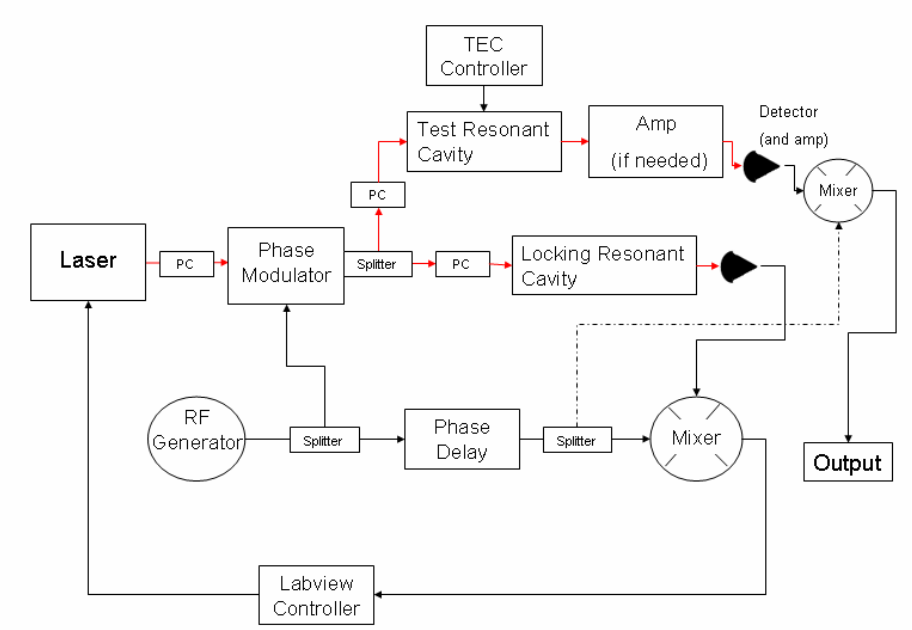

Figure 18 - Dual cavity setup for locking to one cavity and sensing thermal changes using another

Optisystem Model

To approximate the response of the PDH method, the optical and receiver system is setup in Optisystem. This program provides a simulated response of optical filtering and signal analysis. The optical filter here is represented by an inverted Bessel optical filter providing an absorptive cavity with input variables entered to provide a similar response to the Sandia ring resonator. This filter allows cavity linewidth and absorption at resonance to be defined. A schematic of the diagram including error signal filtered DC output is shown in Figure 19. The laser frequency is swept using nine steps to simulate the error signal around resonance.

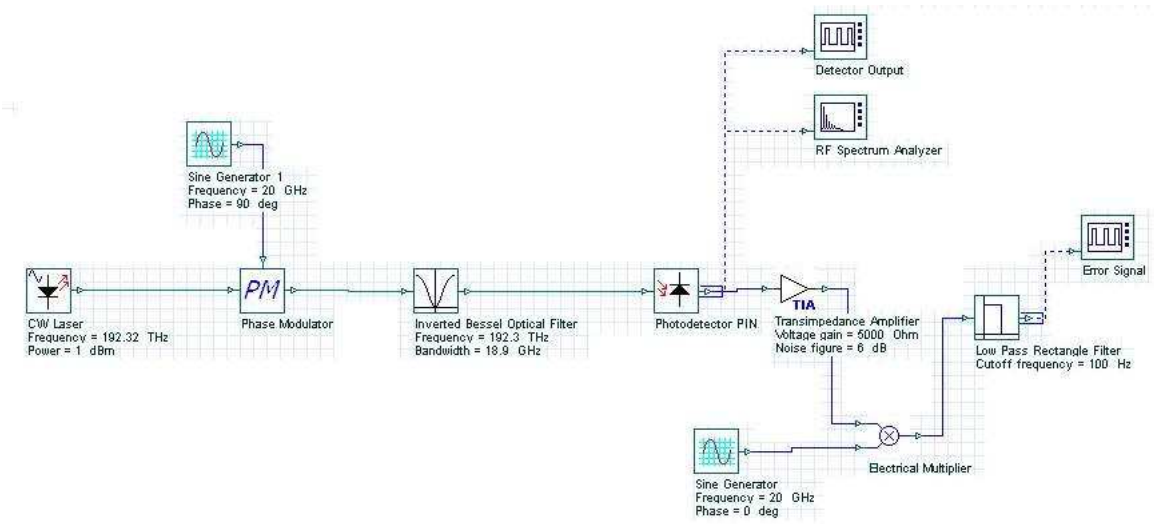

Figure 19- Optisystem model of PDH method

The error signal output is low pass filtered at a 100Hz to find an average for each step as the frequency is swept around the cavity resonance. The values taken for the sweeps are graphed in Figure 20. The error signal is positive when the frequency is lower than resonance and negative when the frequency is greater than resonance.

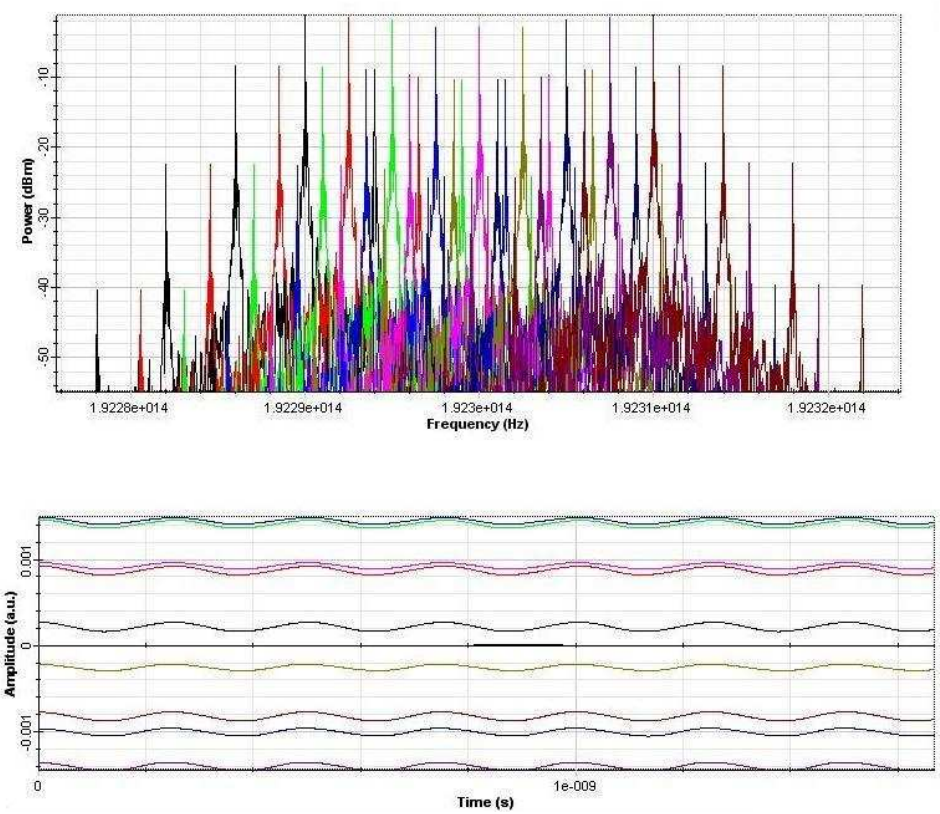

Figure 20- Optisystem optical frequency and resultant error signal after filtering for nine frequencies swept around resonance

The filtered signal does not show extraneous system noise and the only noise simulated is from the modulation frequency signal that is not completely low-pass filtered. There is also an offset at resonance simulating an offset error signal if the DC signal is not filtered after detection. The output shows that around resonance the signal is small and there is opposite polarity dependence for offset frequency. With the math and the optical model in agreement, the output from the ring resonator cavity is expected to have a similar response.

6. ELECTRONIC FEEDBACK

The feedback loop of this experiment starts with the receiver of the optical signal. Two optical high-bandwidth detectors that are able to detect the GHz modulation signal are used. Both detectors filter out DC from the signal and pass up to a tested 4GHz signal for the HP detector and 5GHz for a Picometrix detector. There is a measured output contribution at the modulation second harmonic that is at least 40dB below the main signal.

It is important for the S/N ratio that the signal be amplified before being mixed or filtered. Otherwise, any noise that is added to the system before gain amplification would be also amplified. The signal from the detector is amplified using a series of up to two 14dB RF amplifiers. These are low-noise and rated for the high frequencies incurred from our phase modulation signal. The maximum output power for the RF signal from the detector with this setup is -10dBm input into the RF port of the mixer.

The homodyne mixing is accomplished by a double-balanced mixer. The signal from the detector represents the RF input to the mixer and the LO input is from the RF generator. These are at the same frequency, though at different input amplitudes. The output is an intermediate frequency (IF) signal with significant power out at the 0, φ, and 2 φ frequencies. The error signal is contained in the DC signal and harmonics of the phase modulation signals will add noise to the system if left unmitigated. The IF signal is low-pass filtered using a 1.9MHz LPF block from Mini-Circuits. The resulting DC signal can be displayed on an oscilloscope or sent to the gain feedback controller and control the cavity or the frequency source. In this experiment it can either be sent through a proportional gain block or sent to a Labview controller programmed for PID control. This Labview program also samples the signal and displays the output.

The output from the homodyne mixing is shown in Figure 21 for a 2GHz signal. This also shows the low noise and tight lock of the RF generator signal. The 1.9MHz low pass filter rejection is greater than 45dB for the modulation frequency and other high frequencies are low passed to the noise level.

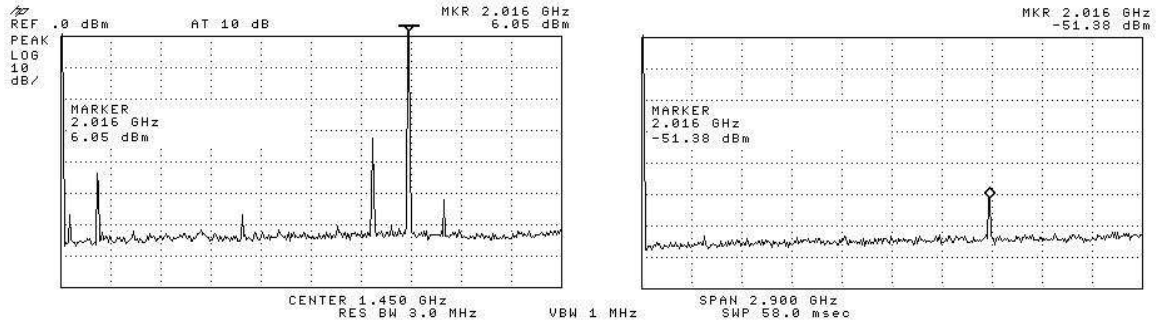

Figure 21- Mixer output signal showing 2GHz noise before and after 1.9MHz LPF

The output from the Labview program and PID controller is low-pass filtered with cutoff at 2.5MHz to filter out extraneous noise from the computer bus architecture that signals off of an 8.3MHz frequency. The system is capable of locking with noise in the feedback frequency higher than 1.9MHz and offset by 1.9MHz around the modulation frequency, but filtering noise before input into the LDC insures that noise signals do not inhibit the current control. The controller output is fed into the LDC to directly control the current of the laser. The control response of the laser is discussed in the optical devices section.

PID Controller

An active compensator is crucial to locking the laser within a quick time limit and holding it at resonance while minimizing the amount of drift and oscillation. This controller allows the laser frequency to track to changes in the cavity resonance frequency. This will minimize noise fluctuations of the laser and track the temperature fluctuations from the device. The device can either be controlled within a temperature range by the TEC or thermally isolated.

A first-order active compensator is able to be used because while locked, the frequency offset from resonance follows a roughly linear slope. If there is any error signal offset, it is predetermined before each lock by slope measurements and corrected for. A PID controller is selected as the active controller because it can easily

compensate for thermal effects to be measured and adjustment between locking results can be quickly compared.

The Ziegler Nichols approach to locking the error signal is used to set the device proportions. First, the critical proportional gain (Ku) is found. To find the critical gain, the integral and derivative gains are set to zero and the proportional gain is increased until standing wave oscillations are achieved in the error signal. The period of this oscillation (Pu) is on the order of a few hundred hertz. This is a higher frequency than the environmental changes of the cavity, so it is determined that the tuning method works without a specific control design needed. The proportional gain (Kp) is set to 0.6 * Ku while the integral gain (Ki) is set to Pu / 2 and the derivative gain (Kd) is set to Pu / 8 [36].

Each sample is multiplied by a gain after comparatively added to the previous input sample and multiplied by an integral and derivative gain. This is defined in Equation 23 for a negative error slope with positive gain values Kp, Ki, and Kd. The result of the error control is considered the pre-output signal. This pre-output signal is added to the previous output value to become the output signal. This last step insures that the laser will track the zero point as the cavity may drift slightly. This is also why the software controller is better for environmental sensing feedback instead of analog feedback electronics. In this equation, $\Delta = V_{in} - V_{previous}$, the comparison of the current sample to the previous sample.

$$V_n = V_{n-1} + K_p * \left[\Delta_i + K_i * \left((\Delta_n - \Delta_{n-1}) + (\Delta_{n-1} - \Delta_{n-2})\right)/2 + K_d * (\Delta_n - \Delta_{n-1})\right] \quad (23)$$

In analog electronics by comparison, a very high bandwidth is obtained, but the output range is limited to tracking the laser frequency over a smaller range and cavity drifts cannot be directly compensated for. The software controller has the ability to store values from previous loops. This creates a way to test different low pass filtering results of the input signal into the program. A tight lock is found for higher sampling rates of

the computer up to a kilohertz, and then higher frequencies cannot be determined to increase the lock noticeably because of the noise from laser linewidth on the cavity lock.

The maximum sampling rate of the program with PID control, and therefore the maximum feedback response of the loop is 2kHz. This limits the period of oscillation able to be measured and compensated for. Because the response of the device is not bandwidth limited, the period of oscillation can be further reduced with a higher bandwidth controller, such as an FPGA controller, to lock higher frequency laser noise. For locking with the DFB laser in this experiment, the PID controller compensates for the measurable frequency drift and provides a better response than the high-bandwidth direct feedback.

7. ERROR SIGNAL OPTIMIZATION

The slope and dynamic range for a cavity error signal around resonance is determined by the cavity design coefficients, laser power, modulation frequency, and the modulation depth. How the modulation depth and frequency influences the slope and frequency range can be chosen to have a fairly flat response around optimum values. The modulation depth is discussed in [12] while the optimum modulation frequency will be discussed here.

The theoretical slopes of different finesse cavities are shown in Figure 22 versus the modulation frequency percentage of the FSR (φ/ν). The optimum modulation frequency is shown in this figure and it will be explained further how to determine this value. The matched and quadrature-phase slopes are both shown in Figure 22 with the quadrature error signal having a larger slope than the real error signal at high modulation frequencies.

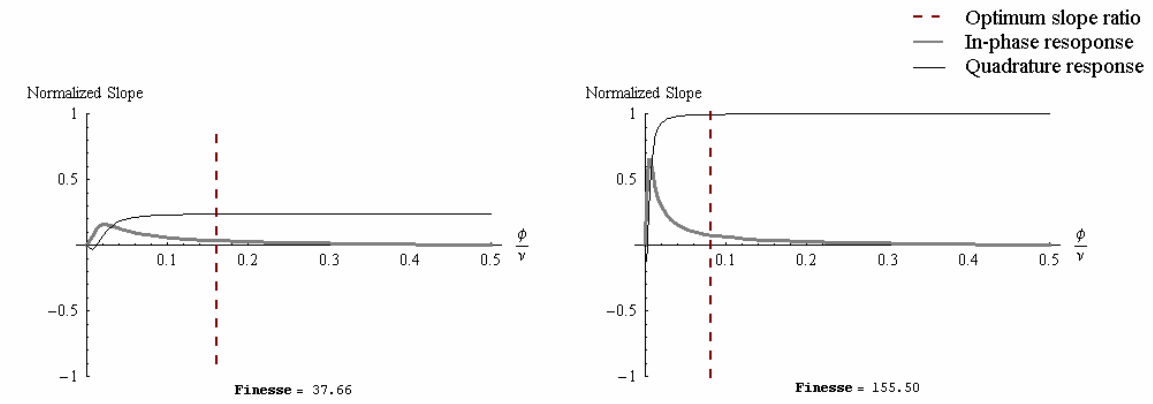

Figure 22 - Optimum slope for varied finesse ring cavities with the optimum modulation ratio shown. These graphs are normalized to the maximum slope when the cavity finesse = 155.5

Optimum Slope at Resonance

The slope of the error signal of amplitude versus frequency shift when the laser is locked on resonance increases the minimum detectable noise from the laser. If the cavity is used for locking a laser frequency, it is beneficial if the phase slope around resonance has been designed to be as large as possible. The resulting error signal slope

around resonance will be large allowing the feedback controller to increase the sensitivity of the lock.

When locked, the variation of laser frequency around resonance is much less than the FSR. For calculations it can also be assumed much less than the phase modulation frequency when locked on cavity resonance. This can be assumed because the modulation frequencies of this experiment are one percent or greater of the FSR whereas the laser frequency variation while locked is less than a few hundredths of a percent of the FSR. The small angle approximation is therefore used to determine the slope immediately around resonance. The resultant slope for a ring resonator cavity from the PDH cavity response is given in Equation 24.

$$\begin{aligned}\text{Re}\quad Slope &= \frac{4\pi\gamma\rho\left(\rho^2-1\right)\left[-1+\gamma\left(2\rho+\gamma(-1+\rho(\rho+\gamma(-2+\gamma\rho)))\right)-2\gamma^2(\rho^2-1)Cos[2\pi y]Sin[2\pi y]\right]}{(\gamma\rho-1)^2\left(1+\gamma^2\rho^2-2\rho\gamma Cos[2\pi y]\right)^2} \\ \text{Im}\quad Slope &= \frac{8\pi\gamma\rho\left(\rho^2-1\right)\left[-1+\gamma\left(-2\rho+\gamma(1+\rho(\rho-\gamma(2+\gamma\rho)))\right)-2\gamma^2(\rho^2+1)Cos[2\pi y]Sin[2\pi y]^2\right]}{(\gamma\rho-1)^2\left(1+\gamma^2\rho^2-2\rho\gamma Cos[2\pi y]\right)^2}\end{aligned} \tag{24}$$

Here the value of $y=\varphi/\nu$, the modulation frequency percentage of the FSR. The transmission coefficients are as defined previously in the optical devices section.

A way to determine an optimum modulation frequency used in the PDH method is necessary in small cavities, because the range between the linewidth and half the FSR can be quite large. The error slope is a direct multiplier to the S/N and increases with higher modulation frequencies. A modulation frequency equal to the linewidth of the cavity has a significant second derivative. This means that the change of the error signal slope is high due to the modulation sidebands not being completely transmitted and coupling and interference occurs between the ring cavity and the sidebands.

Setting the modulation frequency at the value of the linewidth is also the approximate intersection of the real and imaginary slopes. At this frequency, a quadrature phase change between the RF and LO signals into the mixer has a similar slope response and the quadrature signal slope will be approximately 55% of the maximum. This is useful for sensing with a large linewidth cavity, but does not have as good of a S/N ratio for locking. A small amount of error signal amplitude noise results

if the modulation frequency has noise, a matter further discussed in the section on noise. Nonetheless, with a low-noise generating source it is possible to lock onto the error signal with this lower modulation frequency and it has been tested that this is possible.

Though a modulation frequency of half the FSR of the cavity will give the greatest slope, if the device has a high finesse, a slope approaching the maximum error slope is possible with a frequency much less than half the FSR. For a locking cavity this ratio of linewidth to FSR should be very low to achieve a better lock. For a sensing cavity having lower finesse, this method takes into account the challenge of a large linewidth, but the slope increase will still be less than a higher finesse cavity

The following is an optimization to determine the modulation frequency for locking to micro-cavities. An increase in the modulation frequency beyond this optimum frequency will further increase the slope less than four percent its capable maximum. If the linewidth is less than twenty-five percent of the FSR, then an optimum modulation frequency can be found.

If the transmission and coupling coefficients can be determined, an optimum modulation frequency from the slope equations can give a good result. However, magnitude measurements determine the FSR and linewidth of a cavity. Using these two measurements, the optimum modulation for a locking slope is determined from the square root of the linewidth multiplied by the FSR. This is shown in Equation 25 and scales for both the size and coupler/transmission coefficients of the cavity.

$$f_{\mathrm{mod}\,locking} = \sqrt{LW \cdot FSR} \tag{25}$$

This modulation frequency will give at least 96% of the maximum transmission that is obtained from modulating at half the FSR frequency. The ratio of optimization slope to maximum slope is not completely linear over the range of all possible cavities. It approaches one hundred percent of available maximum when the coefficient multiple ($\gamma^*\rho$) is 0.49 and the linewidth approaches half of the FSR or when the coefficient multiple approaches one and the linewidth approaches zero as shown in Figure 23.

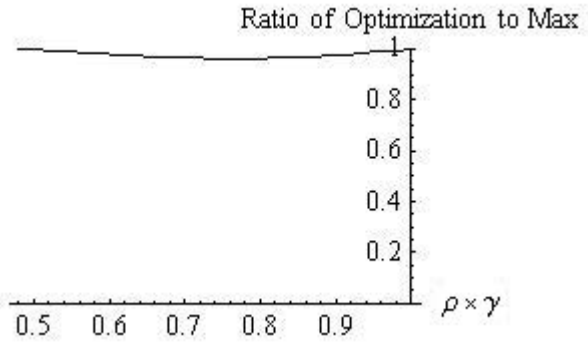

Figure 23 - Modulation frequency optimization compared to the theoretical maximum slope versus the ring resonator coefficient product

Another significant affect on this error slope is the maximum-phase and minimum-phase zero responses. How these affect the error slopes is shown in Figure 24 as a function of the coupling to transmission ratio, or one over the phase zero (z^{-1}). As shown for a set coupling coefficient, the slope decreases as the loss increases. The critical coupling when $\rho/\gamma = 1$ has the largest impact on the transmission intensity at the resonant frequency with the greatest amount of interference at the coupler and diminishing the signal at the through-port. Though, as seen in these graphs, critical coupling does not have the largest impact on the slope of the phase around resonance. The slope is instead maximized for a combination of a maximum-phase zero and also higher coupling coefficients.

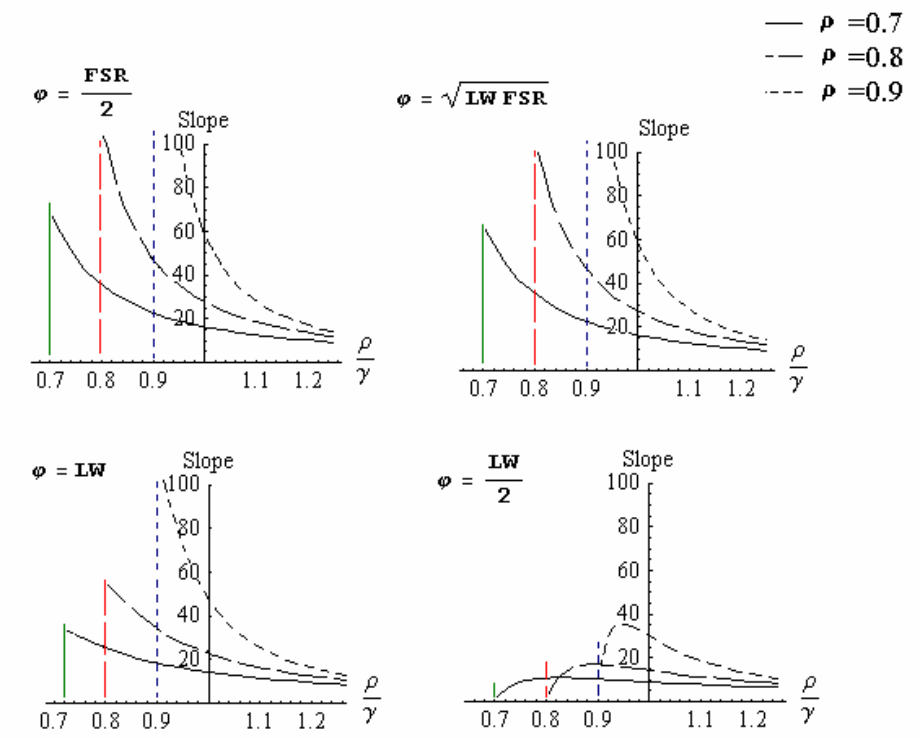

Figure 24- Dependence of the error signal slope locked on resonance versus one over the filter zero (z^{-1}) for various modulation frequencies and coupling coefficients. The modulation frequencies are shown for one-half the FSR, optimum, linewidth, and one-half the linewidth

Optimum Frequency Range

For the case of a sensing cavity, a maximum error signal frequency range can be determined as a linear function of the modulation frequency proportional to the linewidth and coefficient difference. This is obtained by plotting the magnitude of the frequency range between maximum and minimum points of the imaginary error slope around the resonant frequency. The product of the ring coefficients is graphed versus the resulting modulation frequency to maximize the separation between the maximum and minimum values of the imaginary response. The slope of this approximation can be seen in Figure 25.

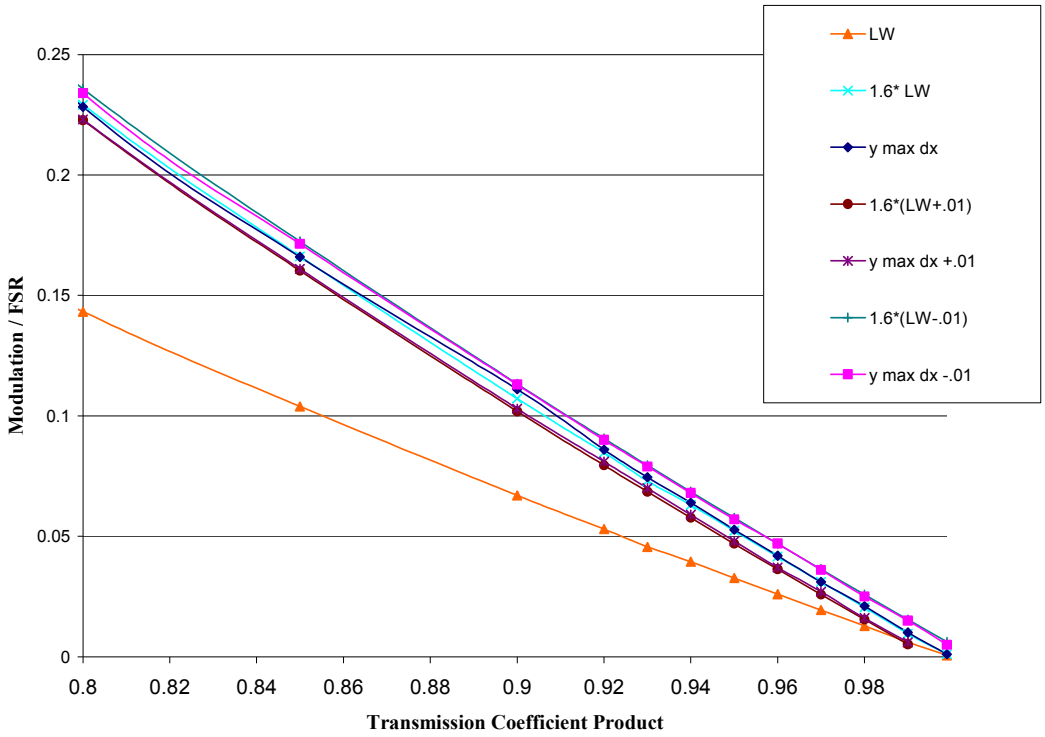

Figure 25 – Modulation frequency as a percentage of the FSR (ymax) to maximize the error signal frequency range (dx)

The approximation is found for the critical coupling case and then for maximum and minimum-phase zero states. It is subsequently found that offset between ρ and γ of 0.01 will change the approximation of the modulation frequency offset one percent of the FSR. Lower modulation frequencies are possible with a minimum-phase filter when $\rho/\gamma > 1$, and are increased for maximum-phase filters. This approximation is linear with the slope of the optimization shown in Equation 26.

$$f_{\mathrm{mod}\,sensor} = 1.6 \times LW \tag{26}$$

The ring resonator coefficients and the FSR have been shown to have a significant influence on the error slope and range around resonance of the ring cavity. The magnitude of the frequency range decreases little as the modulation frequency is

increased greater than the optimum modulation for a sensor. Therefore the optimum slope modulation determined for locking a sensor is better suited to increase both the S/N and the dynamic frequency sensing range. This frequency covers approximately 87% of the maximum frequency range. Conversely, the optimum sensing modulation frequency will induce a slope ranging from 80% to 1% of the maximum slope dependent on the finesse of the cavity.

8. SENSITIVITY RESULTS

Of the integrated single-ring resonators tested in this experiment, the two mentioned in this paper have a large enough finesse to result in an error slope that the laser can be locked onto. This also allows for the experimentation with one cavity as the locking cavity and one as the sensing cavity. The fiber FP cavity sensor has a smaller FSR, but also a significant cavity linewidth so it is better suited for sensing over a large bandwidth. Each ring cavity has one or two resonant frequencies within the frequency tuning range of the laser. The testing between these various cavities as sensors and lock devices allows a greater understanding of the response of these devices.

Slope Results

Slopes are taken with the feedback controller sending a series of small step voltages to the laser over a sweep speed. The sweep rate can be controlled, but greater than 1pm/s gives the best results for the slope. An input sampling rate of 1MS/s was allotted providing many samples per step. With the frequency range of the error signal from the ring resonators, the capable swept range must be at least 4GHz to capture the full error spectrum around resonance.

The cavity phase slope can be estimated from these plots, though the non-linear loss of the microwave components makes it difficult to determine slope before amplification and mixing. The Matlab code to find this approximation is archived in Appendix B. The slope around resonance is first fit with a high-ordered polynomial equation. The center of this slope is then found and the slope is estimated from an average of slope measurements over decreasing fractions of the error signal frequency range. This is an iterative approach because the center may be different than the original fit and the program is rerun with the new center. This method is necessary to find repeatable results because the sampled slope input to the computer is not linear due to its step origin. These slope values were found to be repeatable with less than five percent change between multiple runs.

The Nomadics high-Q ring resonator has the smallest error slope frequency range around resonance, resulting in the largest normalized slope. The slope sweep is shown in Figure 26 with a low, 1GHz modulation. The amplitude change is 90mV and the error slope range is 0.5pm. The corresponding slope is 1.46nV/Hz and has a frequency shift of 680kHz/mV determined from the measurement.

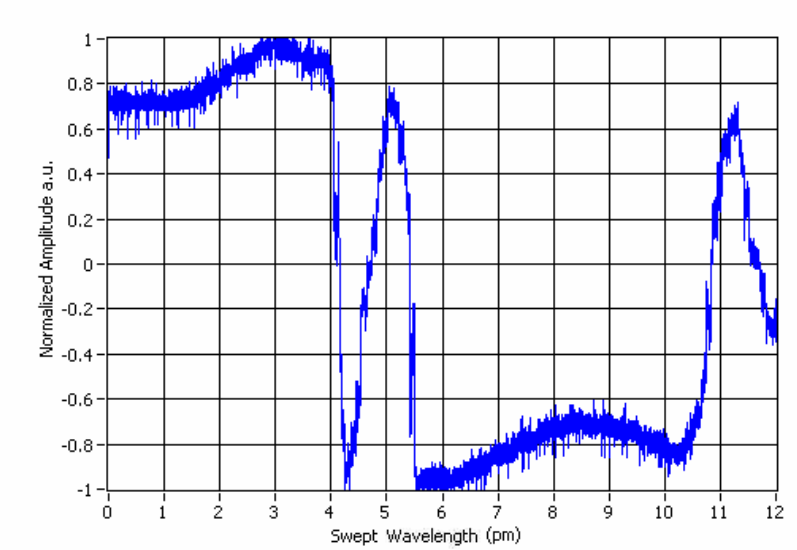

Figure 26- Slope of high-Q Nomadics RR showing the two negative error slopes of the ring due to the double resonance

The Sandia error signal total amplitude before normalization is greater because the optical signal is amplified after passing through the ring resonator. This also proportionally increases the amount of noise as will be evident in the thermal test. The frequency range does not change due to optical amplification and it can be compared to the Nomadics high-Q ring resonator showing the larger linewidth of this cavity. The normalized slope of the Sandia ring resonator is not as steep due to a larger linewidth compared to the Nomadics ring and a greater modulation frequency is needed to receive an error signal with significant slope. This slope for the Sandia ring resonator is shown in Figure 27.

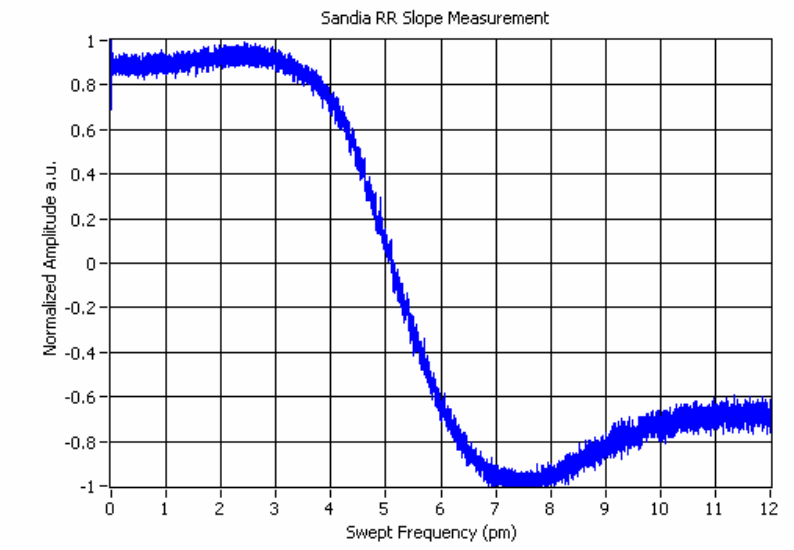

Figure 27 – Slope of the Sandia RR

Locking Results

Locking onto the Nomadics Little Optics ring resonator enables the comparison of the laser noise before and after the lock. The feedback while locked is robust, allowing the lock to hold for a few minutes while taking data and further if experimental data is not needed to be saved. Both a direct feedback gain controller and a PID controller are used for locking comparisons, and each have their own advantages. The response of the PID controller prohibits the laser from losing lock under environmental factors such as tapping on the table next to the device and allows locking if the error signal is not at zero volts output on resonance.

Shown in Figure 28 are two separate locks to the ring resonator established with full PID control and direct feedback. The experiment runs for fifteen seconds without the locking circuit closed. The lock was then turned on for a period of time allowing steady-state measurements and then turned off again to show the laser reverts to a noisy state. The amount of locked noise corresponds to a resolution measurement of about 8MHz, the approximate linewidth of the laser. This is the first lock shown to an integrated ring resonator. The lock can be better achieved with a smaller linewidth laser, enabling a further reduction of the achievable resolution.

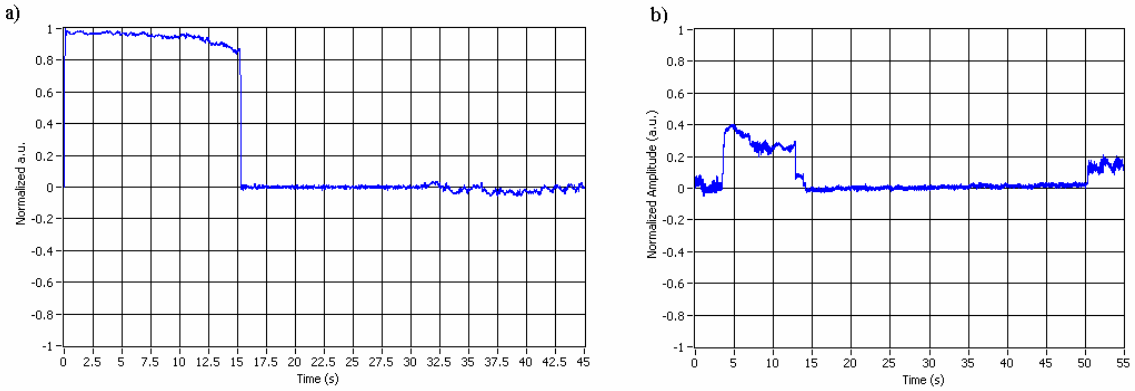

Figure 28- Nomadics high-Q ring resonator feedback locks engaged around 15 seconds and then disconnected after a period of time to show the laser revision to unlocked behavior for a) the PID lock and b) the direct electronics feedback

The PID controlled graph is filtered using a low-pass filter with a cutoff frequency of 500Hz showing the filtered error signal that is sensitive to environmental changes. By comparison, the direct feedback allows the full bandwidth of the electronics sent to the laser controller and the signal is sampled at 100kS/s. In Figure 28 there is a 2mV noise signal and the total amplitude range of the cavity is about 300mV. This locks the laser frequency to less than one percent of the error signal frequency range.

Locking to the Sandia ring resonator and fiber FP cavity can result in a tight lock only if further optical amplification is added to maximize the error slope on either side of resonance. This induces more noise into the error signal and therefore results in a trade-off of locking ability. The laser cannot be locked as tightly as for the Nomadics ring.

The Orbits laser has a linewidth of a few kilohertz, providing the opportunity for a measurement with smaller resolution. The laser sweep and locking resolution for this laser exceeds the locking resolution of the DFB laser at the cost of drifting with the thermal ring effects. The result for this lock is seen in Figure 29 showing the slope and locking of the laser when a separate resonant frequency of the Nomadics ring is thermally tuned into the frequency range. The slope for this laser is 130mV per pm with <0.5% noise measured with a 1kHz low pass filter while locked. The Sandia cavity can not be thermally tuned to this frequency, so the lock is compared to the DFB laser with

the resolution able to be inferred from the resolution of the cavity drift compared to the slope.

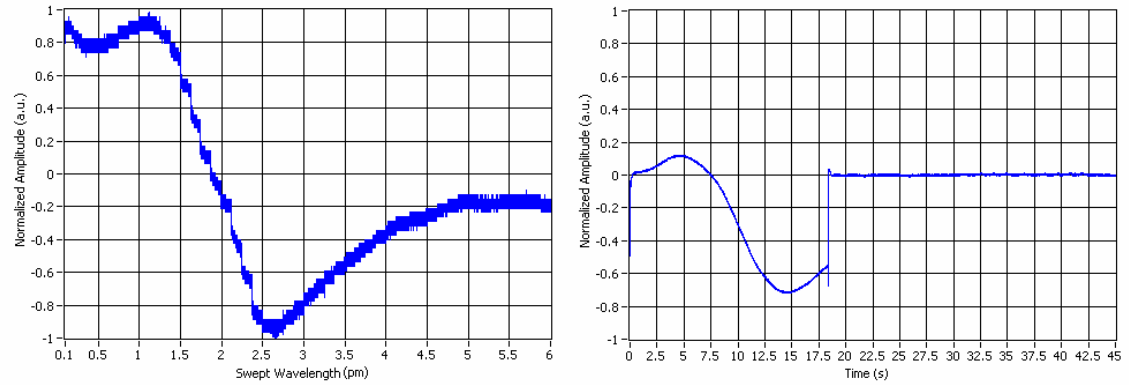

Figure 29 - Orbits laser sweep and lock graphs of the Nomadics ring resonator at two FSR modes away from the DFB locking resonant frequency. The ring here has a single resonant frequency, this difference from the DFB sweep is because it is on a different mode of the cavity

Environmental Test

The Nomadics high-Q ring resonator as discussed has the best locking ability of the cavities tested. For testing purposes, it also helps that the frequency range of the cavity is very small and if lock is lost, it is immediately noted by the abrupt change in the error signal amplitude. The Sandia ring resonator has the next highest finesse of the cavities tested and is used in this experiment to demonstrate sensing of temperature change.

Two TEC units are connected and each ring is setup with a thermistor and Peltier cooler. The Sandia ring resonator is cooled to seven degrees Celsius while the Little Optics resonator is heated slightly above room temperature and both with a measured temperature stability of 0.1 degrees Celsius. The Little Optics high-Q resonator is tuned to be within the error signal bandwidth of the Sandia ring, which is roughly linear. The dependence of the thermal controller setup for Sandia ring resonator is measured by a Finissar laser and detector system to be 4.5pm per 100ohms of resistance of the thermistor.

The result of this experiment shows the error signal of Sandia cavity as the temperature changes. This can be seen in Figure 30 as the cavity is locked after drifting for a few seconds and then the Sandia ring resonant frequency is thermally tuned.

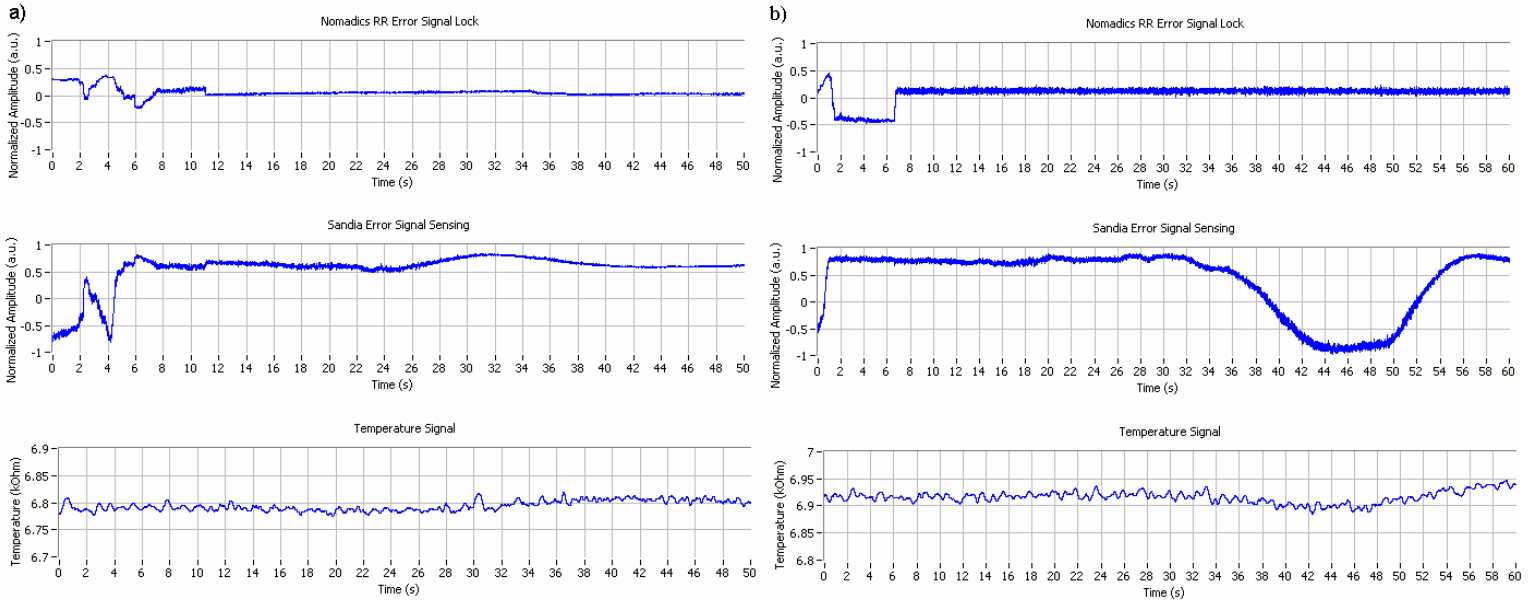

Figure 30 - Environmental affect of temperature on both cavities using a) a PID lock onto the Little Optics cavity and b) a direct feedback lock. In b) the cavity was both heated and then cooled over a 30 second period as can be seen in the dramatic dip of the Sandia RR error signal. The sensitivity of the Sandia cavity can be seen to be much greater than the thermistor

This experiment exemplifies the sensitivity of the ring cavities to be much greater than that of the thermistor. The smallest resolution of shift in wavelength able to be determined by the thermistor is 4.5pm and the error signal resolution from the ring sensor gives a resolution of 0.025 pm, a large increase in sensitivity. Using a fused silica thermal index of refraction of 10.5×10^{-6} this is an estimated shift of 1.9×10^{-8} refractive index units. This demonstrates the ability of the very precise temperature determination that would be important in devices and sensors measuring factors of the environment and sensitive to temperature change.

9. NOISE

A look at the noise caused by the cavities in this experiment and the PDH method is helpful in determining both the results and the benefit of this method. Noise detected at the receiver is shot noise plus laser frequency noise as the signal passes through the cavity. In addition to this, there is noise from the feedback circuit including the RF devices and the PID controller. One advantage of the PDH method is that much of the noise in the system is lower than the modulation frequency and will be filtered out after the homodyne mixer before being sent to the laser current controller.

When locked onto a cavity resonance, the reflected carrier noise is reduced while the sideband amplitude noise predominates. Noise in the optical signal is from laser amplitude fluctuation, noise in the modulation frequency, and cavity noise. One other source of noise, shot noise, does not fall off for frequencies in the GHz modulation range.

The dependence of the error signal on frequency fluctuation (δf) around resonance is determined when locked on resonance. The slope is determined for the ring resonators and FP cavities for both ideal and lossy cases. For noise calculations we will consider the cavity ideal with FP mirror reflection coefficients equal and the loss of the RR cavity negligible. Further, the modulation frequency is set to be half of the FSR to maximize this error slope around resonance. The case when the RF signal is in quadrature with the LO signal will be the Imaginary component of Equation 13 and the slope dependence of the error signal around resonance is then as defined in Equation 27.

$$m_{FP} = -8\pi P_0 J_0 J_1 \frac{R^2}{v_{FP}(R^4 - 1)}$$
$$m_{RR} = -16\pi P_0 J_0 J_1 \frac{\rho}{v_{RR}(\rho^2 - 1)} \tag{27}$$

Here P_0= laser power input and $J_{0,1}$ are Bessel functions of the modulation index. The FSR for each cavity is represented in this equation as ‘ν’. These slopes allow us to look at what is a significant influence of noise in the system. When there is no

frequency offset from resonance, noise in the error signal is immune to the modulation depth, the modulation frequency, and intensity noise of the laser. Frequency noise off of the resonant frequency adds noise proportional to the slope of the cavity error signal.

The lowest level of possible noise in the system occurs when the signal is locked on cavity resonance, approaching the shot noise of the system for a narrow linewidth laser. Shot noise is the electronic noise instability that is the lowest noise threshold using the optic detectors available. It is from the photons striking the photodiode irregularly rather than in a steady flow introducing a random noise into the intensity measurement. While it is difficult to measure the shot noise, it can be estimated. The shot noise for a locked cavity with modulation frequency 50% of FSR has the average power on the detector equal to $2P_s+(P_c-d)$ where d is the amplitude attenuation of the cavity at the resonant frequency. This shot noise is defined as in Equation 28. [12]

$$NS_{elec} = \sqrt{2hf(2P_s + (P_c - d))} \tag{28}$$

In this equation the power of the carrier is, $P_c = J_0^2 P_0$ and sidebands, $P_s = J_1^2 P_0$. The lowest noise possible for these cavities is then represented by the shot noise divided by the slope around resonance for each of the devices.

The slopes for error signals input to the mixer with matched and quadrature phase are shown again in Figure 31. For a low modulation frequency with noise, the slope and therefore the error signal will amplitude modulate and add noise. The noise for the quadrature error signal is determined to add 50% amplitude error slope noise for 1% modulation frequency noise when the modulation frequency is equal to the linewidth, and 0.2% amplitude noise for 1% modulation frequency noise when equal to the optimum modulating frequency. The amplitude modulation is found by adding a one percent offset to the modulation frequency of the slope equation.

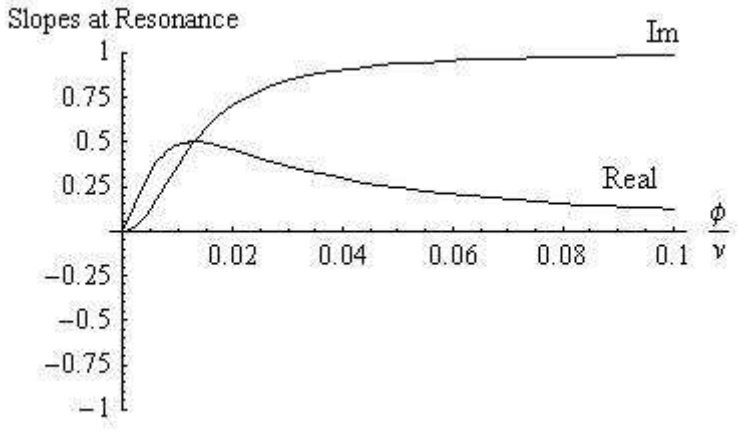

Figure 31- Normalized imaginary and real slopes around resonance, finesse≈100

The noise sensitivity of the computer-controlled PID feedback is also measurable. The input samples per second for the Labview PID controller is set at 2kS/s and a loop is implemented to control the laser current. The Nyquist frequency has a 1kHz cutoff for this loop, so any higher frequency dithering of the laser will be left unhindered. It has been shown in the locking section that low frequency control is effective for locking environmental and low frequency noise of the laser. For the environmental tests it is more important to lock to the resonant frequency and hold it for long periods of time while the sensing cavity is set up and run than to have a feedback signal capable of higher frequency compensation. Direct feedback reduces noise from higher frequencies, but the cavity drifts slightly off of resonance after a few seconds due to slight temperature fluctuations.

The noise level of the error signal limit of detection increases the frequency that must be shifted off of resonance before the amplitude of the light is greater than that of the noise. As discussed, when locked onto a resonant frequency of a cavity, this noise is limited below the approximate linewidth of the DFB laser plus electronic noise from the receiver. Measuring the thermal drift in low frequencies while locked, the laser amplitude noise is mitigated and resolution is largely dependent on the linewidth of the laser utilized.

10. CONCLUSIONS AND FUTURE WORK

It has been shown that integrated ring resonators can be sensitively measured with the Pound-Drever-Hall method. This method uses a high frequency phase modulation and a laser capable of frequency control feedback. Dependent on the frequency of modulation, the PDH method with a high-finesse cavity induces a feedback signal with a steep error curve that can be used to lock a laser to a cavity resonance. Modulating with a frequency larger than the linewidth and much smaller than the FSR allows locking to an integrated micro-ring resonator to be possible.

An approach to ring design was considered to maximize the phase slope around resonance for further improvement in PDH sensing. It was further found that the error slope around resonance increases when ring losses are low, though magnitude response measurements may not indicate this improvement. It was shown that the PDH method would improve sensitivity if a maximum-phase zero was designed for in fabrication of the ring resonator cavity.

A DFB laser and a piezoelectric controlled diode laser were locked to their respective approximate linewidths using a PDH error signal from an integrated ring resonator. The sensitivity of the ring cavity is apparent in locking and sensing measurements. An estimated index of refraction resolution of 1.9×10^{-8} has been found and further resolution is possible with higher finesse cavities and smaller laser linewidths.

There are multiple opportunities for this field as integrated ring resonators can be packaged into small devices, are rugged and very sensitive to environmental affects. Multiple ring resonator cavities and modulation frequencies can be used to scale the sensitivity and frequency range of this method for environmental sensing. Sensing of a resonant frequency shift will depend on the material and environmental affect that is being measured while other changes can be either minimized or taken into account using multiple sensors on the same chip.

The opportunity remains in making even smaller devices and utilizing phase sensing at higher modulation frequencies. Sensing using multiple phase modulations to

determine the environmental affects on single or series of rings will also determine if these devices are robust to multiple environmental affects. Devices made from ring resonators such as modulators, filters, and sensors are likely to make these cavities a continued demand with further improvements in design being made in the future.

REFERENCES

1 A.D. White "Frequency stabilization of gas lasers," *IEEE J. of Quantum Electronics,* vol. 1 no. 8, pp. 349-357, November 1965.

2 R. V. Pound, "Electronic frequency stabilization of microwave oscillators," *The Review of Scientific Instruments*, vol. 17, no. 11, pp. 490-505, November 1946.

3 R.W.P. Drever, J.L. Hall, F.V. Kowalski, J. Hough, G. M. Ford, A. J. Munley, and H. Ward, "Laser phase and frequency stabilization using an optical resonator," *Applied Physics B*., vol. 31, pp. 97-105, June 1983.

4 A. Sollberger, A. Heinamaki, and H. Melchior. "Frequency stabilization of semiconductor lasers for applications in coherent communication systems,". *J. of Lightwave Technology*, vol. LT-5, no. 4, pp. 485-491, April 1987.

5 J. Ye, L.S. Ma, and J. L. Hall, "Ultrastable optical frequency reference at 1.064μm using a C_2HD molecular overtone transition," *IEEE Transactions on Instrumentation and Measurement*, vol. 46, no. 2, pp. 178-182, April 1997.

6 B.C. Young, F.C. Cruz, W. M. Itano, J. C. Bergquist. "Visible lasers with subhertz linewidths," *Physical Review Letters*, vol. 82, no. 19, pp. 3799-3802, May 1999.

7 R.J. Rafac, B.C. Young, F.C. Cruz, J.A. Beall, J.C. Bergquist, W.M. Itano, D.J. Wineland, "$^{199}Hg^{+}$ Optical frequency standard: Progress report*," *1999 Joint Meeting EFTF- IEEE IFCS*, pp. 676-681, 1999.

8 J. Ye, L. S. Ma, and J. L. Hall, "Ultrasensitive detections in atomic and molecular physics: demonstration in molecular overtone spectroscopy," *J. Opt. Soc. Am. B*, vol. 15, no. 1, pp. 6-15, January 1998.

9 A. Yalcin, K. Popat, J. C. Aldridge, T. Desai, J. Hryniewicz, N. Chbouki, B. Little, O. King, V. Van, S. Chu, D. Gill, M. Anthes-Washburn, M. S. Unlu, and B. Goldberg, "Optical sensing of biomolecules using microring resonators," *IEEE J. of Quant. Elec*., vol. 12, no. 1, pp. 148-154, Jan/Feb 2006.

10 I. M. White, H. Oveys, X. Fan, T. L. Smith, J. Zhang, "Integrated multiplexed biosensors based on liquid core optical ring resonators and antiresonant reflecting optical waveguides," *Applied Physics Letters,* vol. 89, p.191106, 2006.

11 S. Arnold, M. Khoshsima and I. Teraoka, "Shift of whispering-gallery modes in microspheres by protein adsorption," *Optics Let*., vol. 28, no. 4, pp. 272-274, Feb. 2003.

12 E. Black, "Notes on the Pound-Drever-Hall technique" *LIGO Technical Note* T980045-00, pp. 1-12, April 1998.

13 T. Bilici, S. Isci, A. Kurt and A. Serpenguzel, "Microsphere-based channel dropping filter with an integrated photodetector," *IEEE Photonics Tech. Let*., vol. 16, no. 2, pp. 476-478, Feb 2004.

14 F. Shen and A. Wang, "Frequency-estimation-based signal-processing algorithm for white-light optical fiber Fabry-Perot interferometers," *Applied Optics*, vol. 44, no. 25, pp. 5206-5214, September 2005.

15 L. Hollberg, J. Aman, S. Waltman, J. H. Marquardt, M. Stephens, R. W. Fox, D.A. Van Baak, C.S. Weimer, H.G. Robinson, A.S. Zibrov, N. Mackie, T.P. Zibrova, and L. Pendrill. "Diode lasers for frequency standards and precision spectroscopy," *Frequency Control Symposium, 49th., Proceedings of the 1995 IEEE International*, pp. 185-189, July 1995.

16 A. E. Siegman, *Lasers*, University Science Books, Mill Valley, California, 1986.

17 R. W. Fox, C. W. Oates, L. W. Hollberg "Stabilizing diode lasers to high-finesse cavities", *Experimental Methods in the Physical Sciences*, vol. 40, Elsevier Science, pp. 1-46, 2003.

18 M. Rakhmanov, M. Evans and H. Yamamoto. "Optical vernier technique for measuring the lengths of LIGO Fabry-Perot resonators," *LIGO Technical Note,* T970174-01, pp. 1-9, 1998.

19 E. M. Lally, "A narrow-linewidth laser at 1550 nm using the Pound-Drever-Hall stabilization technique," M.Sci. Thesis, Virginia Polytechnic Institute, 2006.

20 J. H. Chow, I.C.M. Littler, G. de Vine, D. E. McClelland, and M. B. Gray "Phase-sensitive interrogation of fiber Bragg grating resonators for sensing applications," *J. of Lightwave Technology*, vol. 23, no. 5, pp. 1881-1889, May 2005.

21 J. H. Chow, I.C.M. Littler, D. E. McClelland and M. B. Gray, "Laser noise-limited ultra-high performance remote sensing with a fiber-Fabry-Perot," *Optics Express,* vol. 14, no. 11, pp. 4617-4624, May 2006.

22 T. Day, "Frequency stabilized solid state lasers for coherent optical communications," Ph.D. Dissertation, Stanford University Press, Stanford, CA, 1990.

23 C. K. Madsen, and J. H. Zhao, *Optical filter design and analysis: A signal processing approach*, Wiley, New York, 1999.

24 C. J. Kaalund, and G.D. Peng, "Pole-zero diagram approach to the design of ring resonator-based rilters for photonic applications," *J. of Lightwave Tech*., vol. 22, no. 6, pp. 1548-1559, June 2004.

25 D. G. Rabus, M. Hamacher, U. Troppenz, and H. Heidrich, "Optical filters based on ring resonators with integrated semiconductor optical amplifiers in GaInAsP-InP," *IEEE J. of Selected Topics in Quantum Electronics*, vol. 8, no. 6, pp. 1405-1411, December 2002.

26 O. Schwelb, "Transmission, group delay, and dispersion in single-ring optical resonators and add/drop filters- a tutorial overview," *J. of Lightwave Technology*, vol. 22, no. 5, pp. 1380-1394, May 2004.

27 C.K. Madsen, "General IIR optical filter design for WDM applications using all-pass filters," *J. of Lightwave Technology*, vol. 18, no. 6, pp. 860-868, June 2000.

28 C. D. Cantrell, *Modern mathematical methods for physicists and engineers*, Cambridge University Press, Cambridge, UK, pp. 692-693, 2000.

29 G. Rostami, and A. Rostami, "A new structure for optical integrated digital filters using ring resonators," *IEEE 10th Asia-Pacific Conference on Communications*, pp. 754-759, 2004.

30 J. Guo, M. J. Shaw, G. A. Vawter, P. Esherick, G. R. Hadley, and C. T. Sullivan, "High-Q integrated on-chip micro-ring resonator," *Lasers and Electro-Optics Society, LEOS. The 17th Annual Meeting of the IEEE*, vol. 2, no. 7-11, pp. 745-746, Nov. 2004.

31 M. Thompson, "Fast amplitude and delay measurement for characterization of optical devices," M.Sci. Thesis, Texas A&M University, 2006.

32 Y. Sakai, I. Yokohama, F. Kano, and S. Sudo, "Frequency stabilized laser diode locked to acetylene gas absorption lines using fiber-pigtail-type acoustic optical modulator," *IEEE Photonics Technology Lettters,* vol. 4, no. 1, pp. 96-98, January 1992.

33 L. E. Richter, H. I. Mandelberg, M. S. Kruger, and P. A. McGrath. "Linewidth determination from self-heterodyne measurements with subcoherence delay times," *IEEE J. of Quant. Elect*., vol. QE-22, no. 11, pp. 2070-2074, November 1986.

34 H. Tsuchida, "Simple technique for improving the resolution of the delayed self-heterodyne method," *Optics Letters,* vol. 15, no. 11, pp. 640-642, June 1990.

35 P. Horak and W. Loh, "On the delayed self-heterodyne interferometric technique for determining the linewidth of fiber lasers," *Optics Express,* vol. 14, no. 9, pp. 3923-3928, May 2006.

36 K. Warwick, *An introduction to control systems*, World Scientific, Singapore, pp. 323-324, 1996.

APPENDIX A

LAB PICTURES

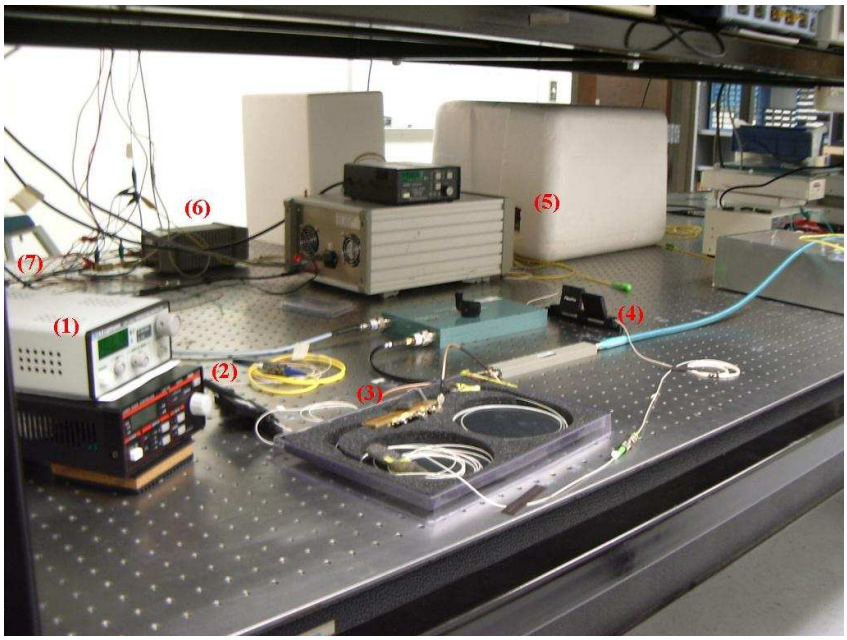

The lab setup from bottom left counter-clockwise. Laser control, polarization controller, phase modulator, polarization controller, optical devices (in Styrofoam housings), detector, mixer. The optical amplifier is the large white housing in the middle of the table with a TEC controller on top. RF phase-shifter and cables are green/blue.

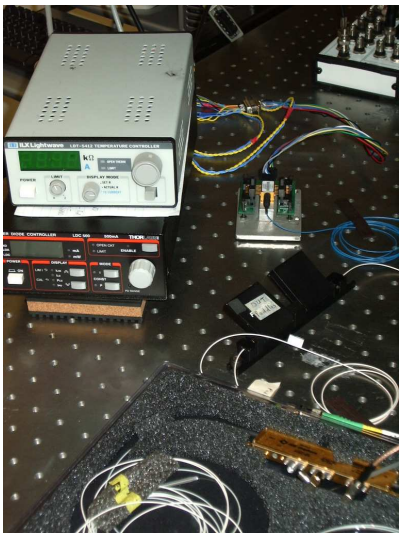

Laser controller with laser diode, polarization controller and phase modulator shown. Feedback is not connected to the LDC in this picture.

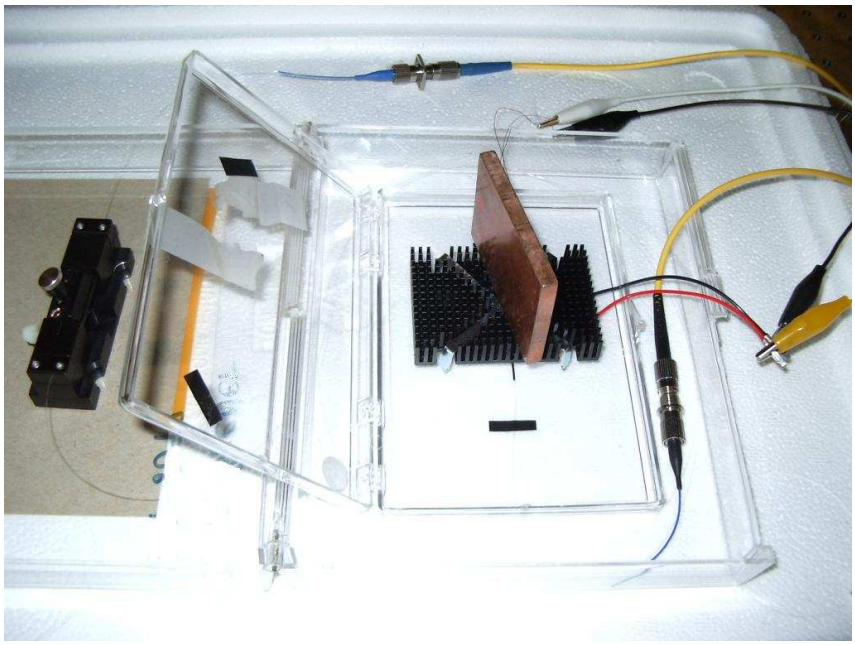

Sandia ring with TEC connections and a polarization controller (left side of picture) connected. The copper block is used for a weight against the spring stand-off of the TEC

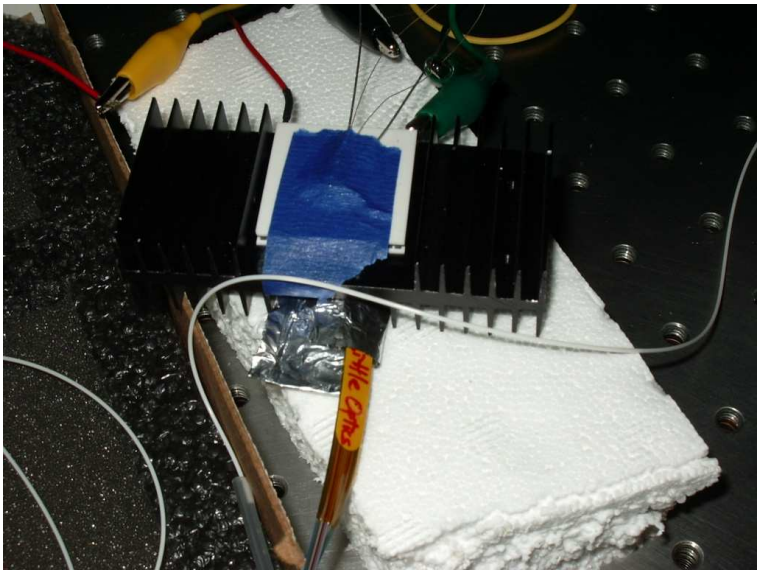

Nomadic's ring resonator from the Little Optics division. In this setup it has been moved from the thermal housing and the TEC is shown connected with the chip containing the ring cavity secured under it. The ring temperature was kept slightly above room temperature and the spacing from the Peltier cooler insured that temperature corrections would be slow.

The Sandia ring resonator chip showing fiber coupling in and out of the chip. The vertical black pieces to the side are tape to hold down the fiber.

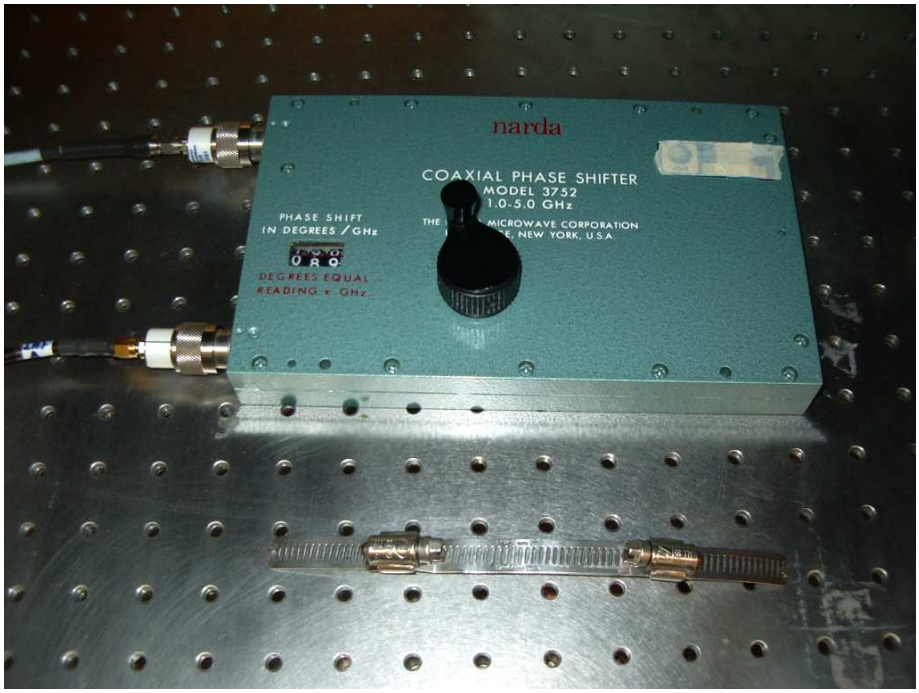

The RF phase modulator above the home-made version that has been removed from its connector housing. Though 50 cents will go a long way (and the results were surprisingly good), the Narda phase shifter had a decidedly lower noise factor in the low GHz range.

APPENDIX B

PROGRAMMED CALCULATIONS

Slope approximation using "fit"

```
%----Truncated Sweep to find the Slope of Blue RR

load 'C:\Documents and Settings\JPC4530\My Documents\Slope
Measurements\Orbitsslope\<Slope runs>.mlv'

figure (2)
plot(running_time*sweep_speed, Opt_pow)
xlabel('Swept Wavelength (pm)')
ylabel('Amplitude (V)')
title(' Sweep Slope Measurement')
grid on


%----------------Slope around resonance

approxcenter= 6.1 ;
approxrange = 0.6;
%frac    = 20;

start=center-approxrange;
finish=center+approxrange;
%samprate=100000;
Istart =round(samprate/sweep_speed*start)   +1 ;

range = (start: sweep_speed/ samprate : finish);
truncPow =  Opt_pow(Istart : round(samprate/sweep_speed* finish));

fit =polyfit(range, truncPow , 12);
fitval= polyval(fit , range);
err = truncPow-fitval;
table = [range truncPow fitval err];

[M, n] = max(fitval);
[O, p] = min(fitval);
maxI= start+n / samprate*sweep_speed
minI = start+p / samprate*sweep_speed


%----------- Output values
for frac=2:10,
  lower = center-abs(minI-maxI)/frac;
  upper = center+abs(minI-maxI)/frac;
  slope(frac)  =
abs(fitval(round((n+p)/2+abs(n-p)/frac))-fitval(round((n+p)/2-abs(n-p)/frac)))
/ abs(upper-lower);
end
```

```
center= (minI+maxI) /2;
slopemean=mean(slope(2:9))
error = mean(abs(err))
center
deltax= abs(maxI-minI)

figure (1)
plot(range,truncPow, range, fitval)
xlabel('Swept Wavelength (pm)')
ylabel('Amplitude (V)')
title('  Laser Slope Approximation Measurement ')
grid on
```

Finding the Beta Ratio from the COSA

```
load 'C:\Documents and Settings\JPC4530\My Documents\CosaCopy\<COSA runs>.mlv'
offset=1000;
n=round(a)
p=round(b)
length(Opt_pow_spect)

lower_spect= Opt_pow_spect(1 : n-offset);
upper_spect= Opt_pow_spect(n+offset : length(Opt_pow_spect));

%[Q, r] = max (lower_spect);
%[S, t]  = max (upper_spect);
%[U, v] = min (lower_spect);
%[W, x]= min (upper_spect);

sum = 0;

for n=1:25 ,
  sideband(n) = (sideband1(n)+sideband2(n)) /2 ;
  BetaRatio(n) =carrier(n) / sideband(n) ;
  sum = BetaRatio(n)+sum;
end

avBetaRatio = sum/n

figure(1)
plot(running_lambda, Opt_pow_spect)
```

C++ dynamic range and slope approximation

```
d#include <iostream>
#include <stdlib.h>
#include <time.h>
#include <math.h>
#include <iomanip.h>

using namespace std;
```

```
int xindex, yindex;
long double num, c, s, v;
const double pi=3.14159265, ychange=.0001, yend=.1, xres=.00001;
const int hold=yend/ychange;
long double maxslope[hold], xlinear[hold], xrange[hold];  ;

void
FabryPerot ()
{
    int refchoice=0, graphchoice=0;
    long double R=0, lw=0, F=0;

    cout << "What information do you have on the fabry perot?\n";
    cout << "1) Total reflectivity\n";
    cout << "2) FWHM linewidth around resonance\n";
    cout << "3) Finesse\n";
    cin  >> refchoice;

    if(refchoice == 1)
    {
       cout << "Please enter the reflectivity of the FP cavity\n";
       cin  >> R;
    }
    else if(refchoice == 2)
    {    cout << "Please enter the linewidth of the FP cavity\n";
         cin  >> lw;
         R= (lw*lw*pi*pi+2*v*v-lw*pi*sqrt(lw*lw*pi*pi+4*v*v))/(2*v*v);
    }
    else if(refchoice == 3)
    {     cout << "Please enter the finesse of the FP cavity\n";
          cin  >> F;
          R=(2*F*F+pi*pi-pi*sqrt(4*F*F+pi*pi))/(2*F*F);
    }

    cout << R << " is the value of the reflectivity coefficient found\n" <<endl;

     cout << "1) Real plot \n";
     cout << "2) Imaginary plot \n";
     cin  >> graphchoice;

     if(graphchoice==1)
     {
        long double numer, denom, replot, replotminus, slope;
        double  x, y=0;

        xrange[yindex]=0;
        xlinear[yindex]=0;
        yindex=1;

        do{
        y=y+ychange;
        xindex=0;
        x=1;
```

```
        x=x-xres;
        maxslope[yindex]=0;
        slope=0;
        numer=4*R*R*(R*R-1)*(R*R-1)*(-R*R*cos(pi*(2*x-y))+(1+R*R+R*R*R*R)*cos(pi*y)-
                R*R*(cos(3*pi*y)+cos(pi*(2*x+y))))*sin(2*pi*x)*sin(pi*y);
        denom=(1+R*R*R*R-2*R*R*cos(2*pi*x))*(1+R*R*R*R-2*R*R*cos(2*pi*(x-
                y)))*(1+R*R*R*R-2*R*R*cos(2*pi*(x+y)));
        replotminus=numer/denom;

        do{
        x=x+xres;
        numer=4*R*R*(R*R-1)*(R*R-1)*(-R*R*cos(pi*(2*x-y))+(1+R*R+R*R*R*R)*cos(pi*y)-
                R*R*(cos(3*pi*y)+cos(pi*(2*x+y))))*sin(2*pi*x)*sin(pi*y);
        denom=(1+R*R*R*R-2*R*R*cos(2*pi*x))*(1+R*R*R*R-2*R*R*cos(2*pi*(x-
                y)))*(1+R*R*R*R-2*R*R*cos(2*pi*(x+y)));
        replot=numer/denom;

        slope=(replot-replotminus)/xres;
        replotminus=replot;
        if(slope>(maxslope[yindex]))     //find maximum slope
        {    maxslope[yindex]=slope;
        }
        if(slope>(maxslope[yindex]*.999)) //find where the slope leaves linearity
        {    xlinear[yindex]=2*(x-1);
        }

        xindex++;
        }while(slope>0);

        xrange[yindex]=2*(x-1-xres);

/*        cout << y << "   is the y value\n";
        cout << "Maximum Slope "<< maxslope[yindex]<< " \n";
        cout << xrange[yindex] << "*FSR full range in x of the slope\n";
        cout << xlinear[yindex] << "*FSR linear range in x of the slope\n"<<endl;
        cout << yindex+1 << " y steps in the loop\n";
*/
        yindex=yindex+1;
        }while(y<yend);
    }

    else if(graphchoice==2)
    {
        long double numer, denom, replot, replotminus, slope;
        double  x, y=0;

        xlinear[yindex]=0;
        xrange[yindex]=0;
        yindex=1;

        do{
        y=y+ychange;
        xindex=0;
```

```
        x=1;
        x=x-xres;
        maxslope[yindex]=0;

        numer=-4*R*R*(R*R-1)*(R*R+1)*sin(2*pi*x)*sin(pi*y)*(sin(pi*y)+R*R*(-sin(pi*(2*x-y))+(-
                2+R*R-2*cos(2*pi*y))*sin(pi*y)+sin(pi*(2*x+y))));
        denom=(1+R*R*R*R-2*R*R*cos(2*pi*x))*(1+R*R*R*R-2*R*R*cos(2*pi*(x-
                y)))*(1+R*R*R*R-2*R*R*cos(2*pi*(x+y)));
        replotminus=numer/denom;

        do{
        x=x+xres;
        numer=-4*R*R*(R*R-1)*(R*R+1)*sin(2*pi*x)*sin(pi*y)*(sin(pi*y)+R*R*(-sin(pi*(2*x-y))+(-
                2+R*R-2*cos(2*pi*y))*sin(pi*y)+sin(pi*(2*x+y))));
        denom=(1+R*R*R*R-2*R*R*cos(2*pi*x))*(1+R*R*R*R-2*R*R*cos(2*pi*(x-
                y)))*(1+R*R*R*R-2*R*R*cos(2*pi*(x+y)));
        replot=numer/denom;

        slope=(replot-replotminus)/xres;
        replotminus=replot;

        if(slope>maxslope[yindex])     //find maximum slope
        {    maxslope[yindex]=slope;
        }
        if(slope>maxslope[yindex]*.999)//find where the slope leaves linearity
        {    xlinear[yindex]=2*(x-1);
        }

        xindex++;
        }while(slope>0);

        xrange[yindex]=2*(x-1-xres);

        cout << y << "   is the y value\n";
        cout << "Maximum Slope "<< maxslope[yindex]<< " \n";
        cout << xrange[yindex] << "*FSR full range in x of the slope\n";
        cout << xlinear[yindex] << "*FSR linear range in x of the slope\n"<<endl;
//        cout << yindex+1 << " y steps in the loop\n";

        yindex++;
        }while(y<yend);
    }
}

void
RingRes ()
{
    int refchoice=0, graphchoice=0;
    long double R=0, lw=0;

    cout << "What information do you have on the ring resonator?\n";
    cout << "1) Transmission efficiency\n";
    cout << "2) FW/BW linewidth around resonance\n";
```

```
//    cout << "C) Finesse\n";
    cin  >> refchoice;

    if(refchoice == 1)
    {
       cout << "Please enter the transmission gain of the RR cavity\n";
       cin  >> R;
    }
    else if(refchoice == 2)
    {    cout << "Please enter the linewidth of the RR cavity\n";
       cin  >> lw;
       R= (lw*lw*pi*pi+2*v*v-lw*pi*sqrt(lw*lw*pi*pi+4*v*v))/(2*v*v);
    }
/*    else if(refchoice == 'c'||refchoice=='C')
       cout << "Finesse equivalent unknown";
*/

    cout << R << " is the value of the transmission absorption found\n" <<endl;


    cout << "1) Real plot \n";
    cout << "2) Imaginary plot \n";
    cin  >> graphchoice;

    if(graphchoice==1)
    {
       long double numer, denom, replot, replotminus, slope;
       double  x, y=0;

       xlinear[yindex]=0;
       xrange[yindex]=0;
       yindex=1;


       do{
       y=y+ychange;
       xindex=0;
       x=1;
       x=x-xres;
       maxslope[yindex]=0;

       numer=-2*R*(R*R-1)*(R*R-1)*sin(2*pi*y)*(-2*sin(2*pi*x)+sin(2*pi*(x-y))+sin(2*pi*(x+y)));
       denom=(1+R*R-2*R*cos(2*pi*x))*(1+R*R-2*R*cos(2*pi*(x-y)))*(1+R*R-2*R*cos(2*pi*(x+y)));
       replotminus=numer/denom;

            do{

              x=x+xres;
              numer=-2*R*(R*R-1)*(R*R-1)*sin(2*pi*y)*(-2*sin(2*pi*x)+sin(2*pi*(x-
                y))+sin(2*pi*(x+y)));
              denom=(1+R*R-2*R*cos(2*pi*x))*(1+R*R-2*R*cos(2*pi*(x-y)))*(1+R*R-
                2*R*cos(2*pi*(x+y)));
              replot=numer/denom;
```

```
            slope=(replot-replotminus)/xres;
            replotminus=replot;
            if(slope>maxslope[yindex])     //find maximum slope
            {    maxslope[yindex]=slope;
            }
        if(slope>maxslope[yindex]*.999)//find where the slope leaves linearity
        {    xlinear[yindex]=2*(x-1);
        }

        xindex++;
        }while(slope>0);

        xrange[yindex]=2*(x-1-xres);

/*        cout << y << "   is the y value\n";
        cout << "Maximum Slope "<< maxslope[yindex]<< " \n";
        cout << xrange[yindex] << "*FSR full range in x of the slope\n";
        cout << xlinear[yindex] << "*FSR linear range in x of the slope\n"<<endl;
        cout << yindex+1 << " y steps in the loop\n";
*/

        yindex++;
        }while(y<yend);
    }

    else if(graphchoice==2)
    {
        long double numer, denom, replot, replotminus, slope;
        double  x, y=0;

        xlinear[yindex]=0;
        xrange[yindex]=0;
        yindex=0;

        do{
        y=y+ychange;
        xindex=0;
        x=1;
        x=x-xres;
        maxslope[yindex]=0;

        numer=2*R*(-1+R*R)*(-2*R*cos(2*pi*x)+(1+R*R)*cos(2*pi*y))*(2*sin(2*pi*x)-sin(2*pi*(x-y))-
                sin(2*pi*(x+y)));
        denom=(1+R*R-2*R*cos(2*pi*x))*(1+R*R-2*R*cos(2*pi*(x-y)))*(1+R*R-2*R*cos(2*pi*(x+y)));
        replotminus=numer/denom;

            do{
              x=x+xres;
              numer=2*R*(-1+R*R)*(-2*R*cos(2*pi*x)+(1+R*R)*cos(2*pi*y))*(2*sin(2*pi*x)-
                 sin(2*pi*(x-y))-sin(2*pi*(x+y)));
              denom=(1+R*R-2*R*cos(2*pi*x))*(1+R*R-2*R*cos(2*pi*(x-y)))*(1+R*R-
                 2*R*cos(2*pi*(x+y)));
```

```
            replot=numer/denom;

            slope=(replot-replotminus)/xres;
            replotminus=replot;
            if(slope>maxslope[yindex])     //find maximum slope
            {    maxslope[yindex]=slope;
            }
        if(slope>maxslope[yindex]*.999)//find where the slope leaves linearity
        {    xlinear[yindex]=2*(x-1);
        }

        xindex++;
        }while(slope>0);

        xrange[yindex]=2*(x-1-xres);

/*          cout << y << "   is the y value\n";
        cout << "Maximum Slope "<< maxslope[yindex]<< " \n";
        cout << xrange[yindex] << "*FSR full range in x of the slope\n";
        cout << xlinear[yindex] << "*FSR linear range in x of the slope\n"<<endl;
        cout << yindex+1 << " y steps in the loop\n";
*/
        yindex++;
        }while(y<yend);
      }
}

void
FindMaxSlope()
{
    long double priormax=0,halfmax=0,nearmax=0;
    int maxholder,halfholder,nearholder;

    for(int i=0;i<((yend/ychange));i++)
    {
     if(maxslope[i]>priormax)
     {     priormax=maxslope[i];
           maxholder=i;
     }
    }
    for(int j=0;j<(yend/ychange);j++)
    {     if((maxslope[j]<maxslope[maxholder]*.5)&&(maxslope[j+1]>maxslope[maxholder]*.5))
          {  halfmax=maxslope[j];
             halfholder=j;
          }
          if((maxslope[j]<maxslope[maxholder]*.99)&&(maxslope[j+1]>maxslope[maxholder]*.99))
          {  nearmax=maxslope[j];
             nearholder=j;
          }
    }
    cout<<"Halfmax "<<halfmax<<" at "<<(halfholder+1)*ychange<<" linear region
                "<<xlinear[halfholder+1]<<endl;
```

```
    cout<<"Nearmax "<<nearmax<<" at "<<(nearholder+1)*ychange<<" linear region
                "<<xlinear[nearholder+1]<<endl;
    cout<<"Maxslope "<<priormax<<" at "<<(maxholder+1)*ychange<<" linear region
                "<<xlinear[maxholder+1]<<endl;
}

void
Closing()
{
        int close;
          cout << "End of program\n";
          cin  >> close;
}

int main ()
{
int choice=0;

    do{
       cout << setprecision(9) << "Enter the FSR of the cavity in Hz\n";
       cin  >> v;
       cout << "Please choose the cavtiy to be calcuated\n";
       cout << "1)  Fabry Perot cavity\n";
       cout << "2)  Ring Resonator cavity\n";
       cout << "3)  enter 3 to quit\n";
       cin  >> choice;

       if(choice==1||choice==2)
       {
           if(choice ==1)
           {  FabryPerot ();
           }
           if(choice ==2)
           {  RingRes ();
           }
           cout <<"Slope Equations complete\n";
           FindMaxSlope();
       }
       if(choice==1||choice==2||choice==3)
           cout<<"\n Done for now?\n ----------------------\n\n";
       else
       {cout << "Choice was not 1 or 2\n" <<endl;
       }
    }while(choice!=3);

    Closing();
    return 0;
}
```

VITA

Name:	James Paul Chambers
Address:	c/o Electrical Engineering Department
	100 Zachry Building
	College Station, TX 77843-3128
Email Address:	JPauls.Ebox@gmail.com
Education:	B.S. Engineering Physics, Colorado School of Mines, 2005
	M.S. Electrical Engineering, Texas A&M University, 2007